Solid state NMR Spectroscopy

Structural Biology (LS5648)
Department of Life Science,
National Tsing Hua University

Instructor : Der-Lii M. Tzou
tzou@ccvax.sinica.edu.tw
Hours: 9:00-12:00 am on March 29, 2006

Course content

1. Introduction to solid state NMR
2. Nuclear Spin and magnetization
3. Pulsed NMR and Fourier transform NMR
4. Anisotropic Interaction in solid: CSA, dipolar, and quadrupolar interaction)
5. Cross-polarization (CP) and Magic Angle Spinning (MAS)
6. 2H, 13C, 15N, 31P NMR spectroscopy and multi-dimensional NMR
7. Molecular Orientation and Anisotropy interaction
8. Applications of solid-state NMR to Membrane proteins and β–amyloid fibril proteins related to Alzheimer's disease

Structured approach bags chemistry prize

David Adam, London

Discerning the shape and structure of biomolecules is a sizeable problem — huge, complicated structures such as proteins are among the toughest molecules to analyse. Three researchers who developed key tools to study these giants have been rewarded with the Nobel Prize in Chemistry.

Half of the prize goes to Kurt Wüthrich of the Swiss Federal Institute of Technology in Zürich and the Scripps Research Institute in California, for finding ways to determine the three-dimensional structures of large biological molecules using nuclear magnetic resonance (NMR) spectroscopy.

John Fenn of the Virginia Commonwealth University in Richmond and Koichi Tanaka of the Shimadzu Corporation in Kyoto share the other half for inventing techniques to identify and analyse proteins and other large structures using mass spectrometry. At 43, Tanaka is the youngest chemistry laureate since 1967, and the second Japanese scientist to receive a Nobel this year, following physics winner Masatoshi Koshiba.

"The possibility of analysing proteins in detail has led to increased understanding of the processes of life," says the Nobel Foundation. "Researchers can now rapidly and simply reveal what different proteins a sample contains and also determine what protein molecules look like in solution."

Broad spectrum: techniques devised by (from left) Koichi Tanaka, John Fenn and Kurt Wüthrich have helped to reveal the secrets of protein structure.

Chemists have used NMR and mass spectrometry for decades to study small molecules. But the large size and complex structure of proteins posed problems for biologists wanting to do the same.

NMR analyses the way a molecule's atoms absorb radio waves in a powerful magnetic field. Proteins can contain thousands of atoms, so they give highly confusing NMR spectra. But in the 1980s, Wüthrich showed that NMR is possible for proteins. He invented 'sequential assignment' in which he determined the distance between any two hydrogen atoms in the molecule. He could then pair each peak of radio absorption with a hydrogen nucleus in the protein. This allowed the structure of proteins to be determined in the form in which they exist in the body — in solution — rather than as crystals.

Mass spectrometry is a highly sensitive analytical tool that separates molecules according to their size. Fenn and Tanaka found ways of turning proteins into a charged vapour, to be accelerated by an electric field and detected in a mass spectrometer.

Tanaka's technique — soft laser desorption — uses a laser pulse to blast material from solid or viscous biological samples. Fenn developed a different approach, electrospray ionization, which creates a fine spray from a protein solution using an electric field.

Fenn has "been in a total state of shock" since being given the news in a dawn phone call on 9 October. "It's like being struck by lightning," he says. "You know it happens to some people but the odds are so great you never believe it will happen to you." ■

Nobel Laurents related to NMR

2003	P. C. Lauterbur and P. Mansfield in Medicine
2002	Kurt Wüthrich in Chemistry
1991	Richard R. Ernst in Chemistry
1952	Felix Block and E. M. Purcell in Physics


AVANCE 400

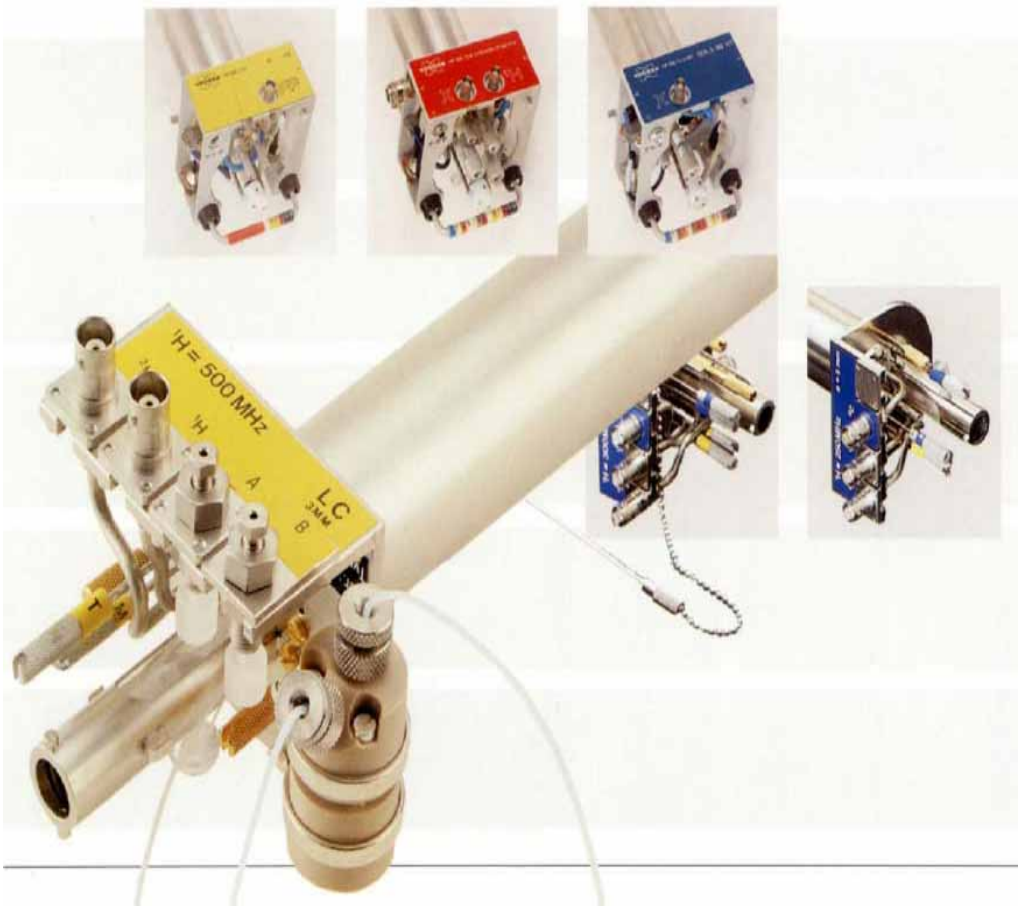
1H = 500 MHz
1H
A
LC
3MM
B

Number of spin states (2I +1) :

A nucleus with spin I can have 2I +1 spin states. Each of these states has its own spin quantum number m (m = − I, −I +1,…, I −1, I). For nuclei with I =1/2, only two states are possible : m = +1/2 and m = −1/2.

Nuclear Zeeman effect :

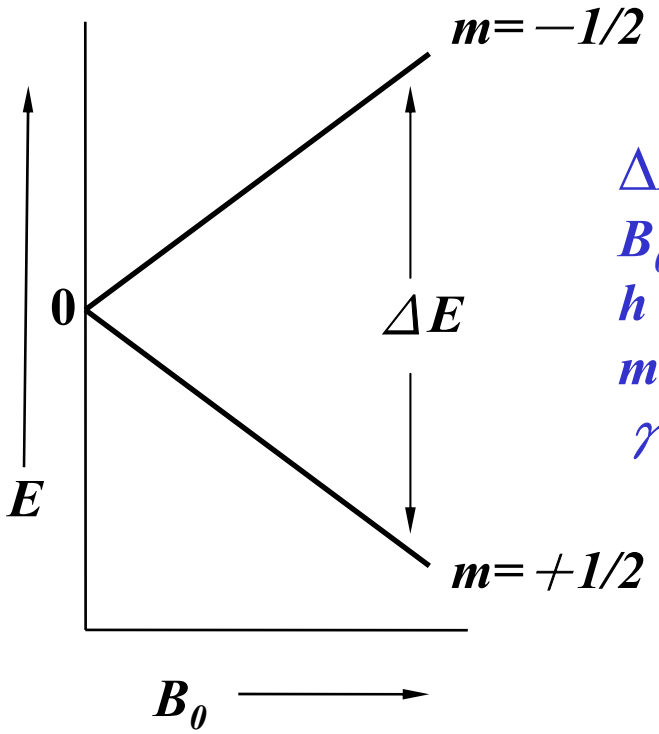

$\Delta E = -B_0(\gamma h/2\pi)$

B_0 : magnetic field strength

h : Planck's constant

m : spin quantum number

γ : magnetogyric ratio

(a) Nuclear spin and Larmor frequency

Nuclear spin (I) :

$$A = Z + N$$

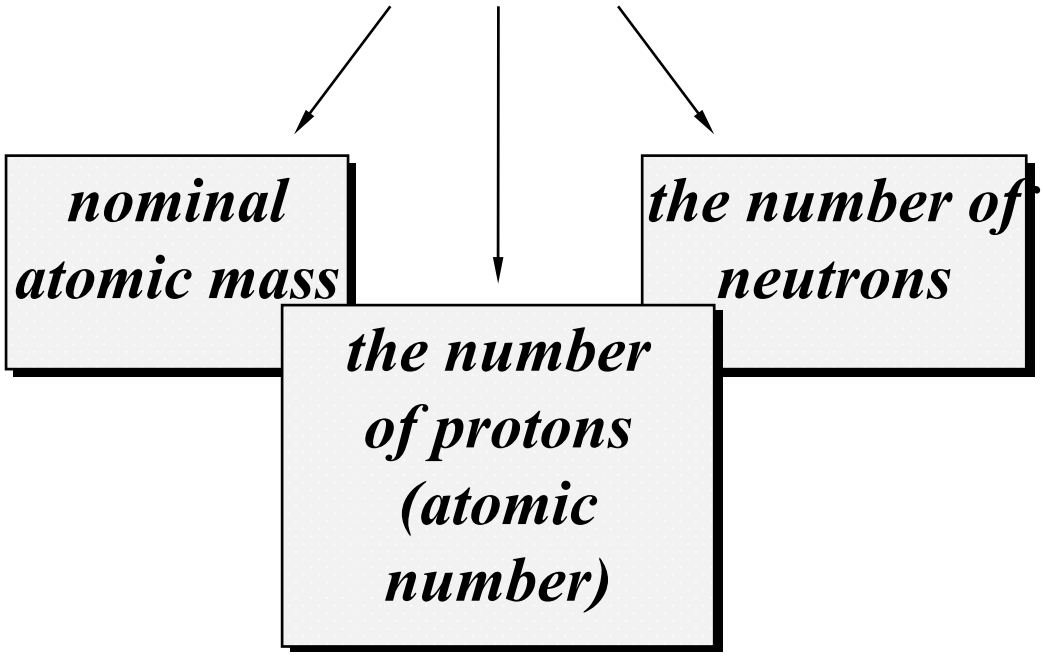

A nucleus with an even mass A and even charge Z, and therefore also an even N, will have a nuclear spin I of zero. (^{12}C, ^{16}O, and ^{18}O).

$$N + Z\,(P) = A$$

$$\left.\begin{aligned} {}^{12}C:\ 6 + 6\,(6) &= 12 \\ {}^{16}O:\ 8 + 8\,(8) &= 16 \end{aligned}\right\} \quad I = 0$$

A nucleus with an even mass and odd charge (both Z and N odd) will exhibit an integer value of I. ($^{2}H(I=1)$, $^{14}N(I=1)$, and $^{10}B(I=3)$)

$$\left.\begin{aligned} {}^{14}N:\ 7 + 7\,(7) &= 14 \\ {}^{2}H\ :\ 1 + 1\,(1) &= 2 \end{aligned}\right\} \quad I = 1$$

A nucleus with odd mass (Z odd and N even, or Z even and N odd) will have nuclear spin with an I value that we can express as n/2, where n is an odd integer. ($^{1}H(I=1/2)$, $^{13}C(I=1/2)$, and $^{17}O(I=5/2)$)

$$\left.\begin{aligned} {}^{1}H:\ 0 + 1\,(1) &= 1 \\ {}^{13}C:\ 7 + 6\,(6) &= 13 \end{aligned}\right\} \quad I = 1/2$$

- ***Nuclei with $I = 0$ cannot be detected by NMR.***
- ***Nuclei with $I \neq 0$ can be detected by NMR.***
- ***Different isotopes of the same element have different nuclear spins, some are detectable by NMR, some are not.***

Properties of important nuclei in NMR studies of protein

Isotope	Spin	Frequency (MHz) at 11.74 T	Nature abundance(%)	Relative sensitivity
^{1}H	1/2	500.0	99.98	1.00
^{2}H	1	76.7	1.5×10^{-2}	9.65×10^{-3}
^{3}H	1/2	533.3	0	1.21
^{12}C	0	------	98.89	------
^{13}C	1/2	125.7	1.108	1.59×10^{-2}
^{14}N	1	36.1	99.63	1.01×10^{-3}
^{15}N	1/2	50.7	0.37	1.04×10^{-3}
^{16}O	0	------	~100	------
^{17}O	5/2	67.8	3.7×10^{-2}	2.91×10^{-2}
^{19}F	1/2	470.4	100	0.83
^{31}P	1/2	202.4	100	6.63×10^{-2}

Larmor Frequency

$$\Delta E = \gamma \hbar B_0 = h\nu$$

$$\nu = \frac{\gamma}{2\pi} B_0$$

(b) Rotation spectroscopy

A classical description of Larmor Frequency

Any motion of a charged particle has an associated magnetic field; on a macroscopic scale an electrical current, which is due to motion of electron along a conductor, produces such a field. Current traveling in a loop has an associated magnetic dipole moment. This phenomenon also occurs on an atomic scale, for whenever electrons or nuclei possess angular momentum there is a magnetic moment. Since angular momentum is quantized on this scale, so are magnetic moments.

Suppose an electron is traveling in an orbit at an angular velocity ω. Such motion is equivalent to an electrical current in the opposite direction of magnitude $i = e\omega/2\pi$, where e is the magnitude of the charge on the electron.

The orbital angular momentum, denoted P, is $m_e r^2 \omega$ where m_e is the mass of the electron and r its distance from the nucleus.

Thus, the current is

$$i = e\omega/2\pi = eP/2\pi m_e r^2$$

The magnetic moment μ generated by such motion is given in electromagnetic theory by $\mu = Ai$, where A is the area marked out by the orbital. $A = \pi r^2$

$$\mu = -(e/2m_e)P$$

Normally, nuclear magnetic moments are described in terms of magnetogyric ratio γ. The γ value of is defined as the ratio of the magnetic moment, P, to the angular momentum, μ.

$$\mu = \vec{\gamma} P$$

In the presence of a magnetic field B_o the energy of an isolated nucleus is dependent of the quantum number m_I.

In classical terms, an energy U given by

$$U = - \vec{\mu} \cdot \vec{\mathbf{B}} = - \mu_z B_o$$

$$= - \gamma \hbar m_I B_o$$

$$\Delta E = E_{+1} - E_{-1} = -\gamma \hbar B_o$$

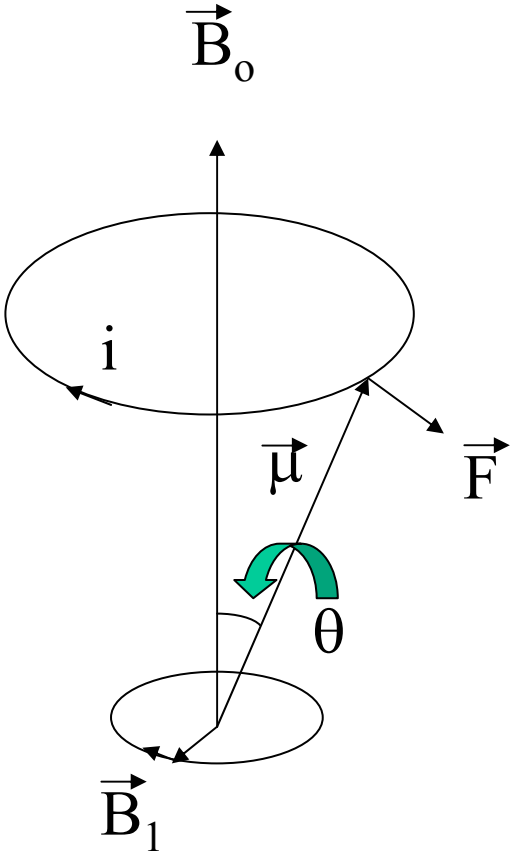

Suppose there is an additional weak magnetic field, B_1, perpendicular to B_o. Such a field will also exert a torque on μ, tending to change the angle θ between μ and B_o. However, if B_1 is fixed in direction it will alternately try to increase and decrease θ as μ precesses. Since B_1 is stated to be weak, the net effect will be a slight wobbling in the precession of μ; such an effect is referred to as nutation. Alternatively, the motion of μ can be described as caused by a resultant field $B_o + B_1$. If, on the other hand, B_1 is not fixed in direction, but is rotating about B_o with the same frequency as the precession of μ and in the same direction, its orientation with respect to μ will be constant. Suppose this orientation is such that B_1 is always perpendicular to the plane containing B_o and μ, then the torque exerted on μ by B_1 will always be away from B_o. Consequently, a large effect on μ is possible. Since changing θ corresponds to changing the energy of μ in B_o, this condition is described as resonance-the frequency, υ, of the field B_1 required must equal the Larmor precession frequency.

Without External Magnetic Field

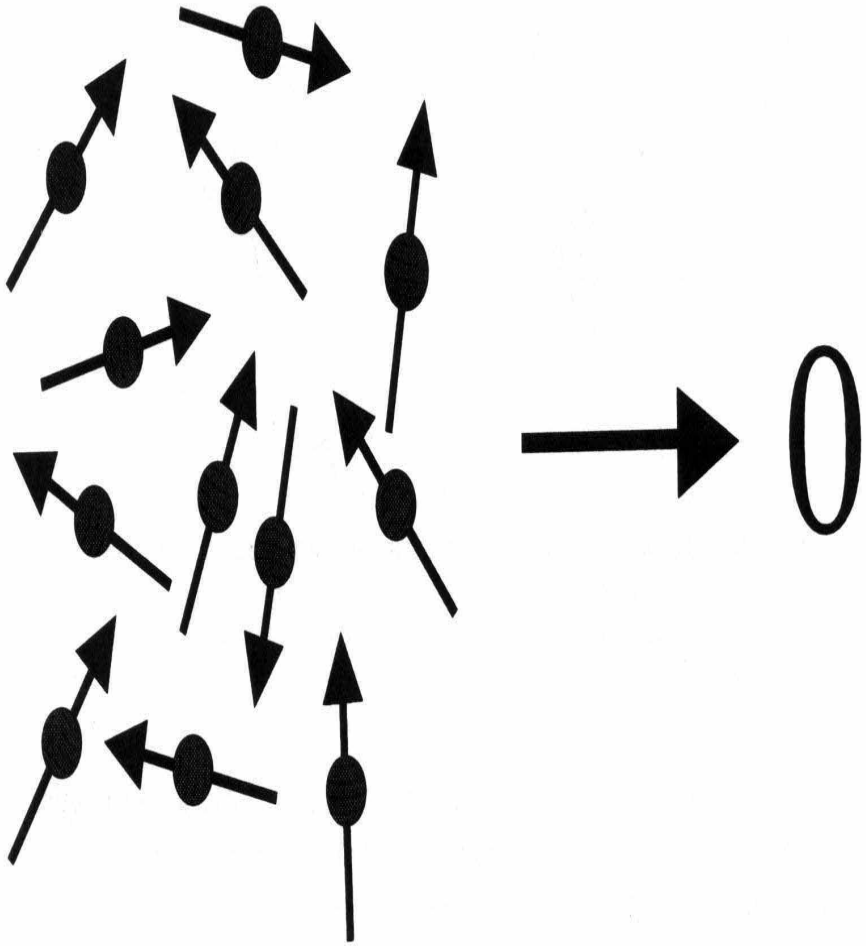

Figure 2.2. Microscopic picture and macroscopic picture of a collection of spins in the absence of an external magnetic field. In the absence of a magnetic field, the spins will have their spin vectors oriented randomly (microscopic picture). The vector sum of these spin vectors will be zero (macroscopic picture).

With External Magnetic Field

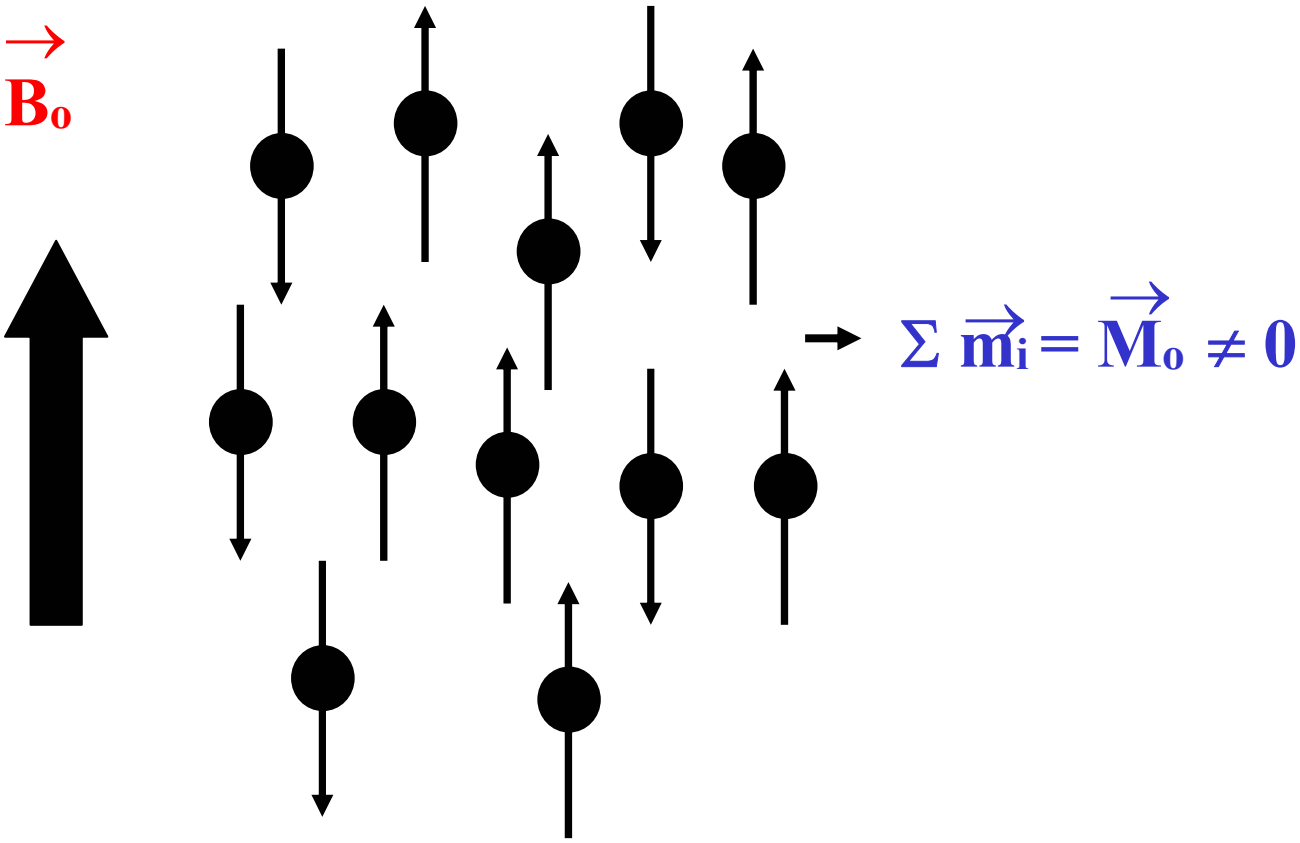

$$\vec{B}_o \gg \vec{M}_o$$

Energy States for I = 1/2, 1, 3/2

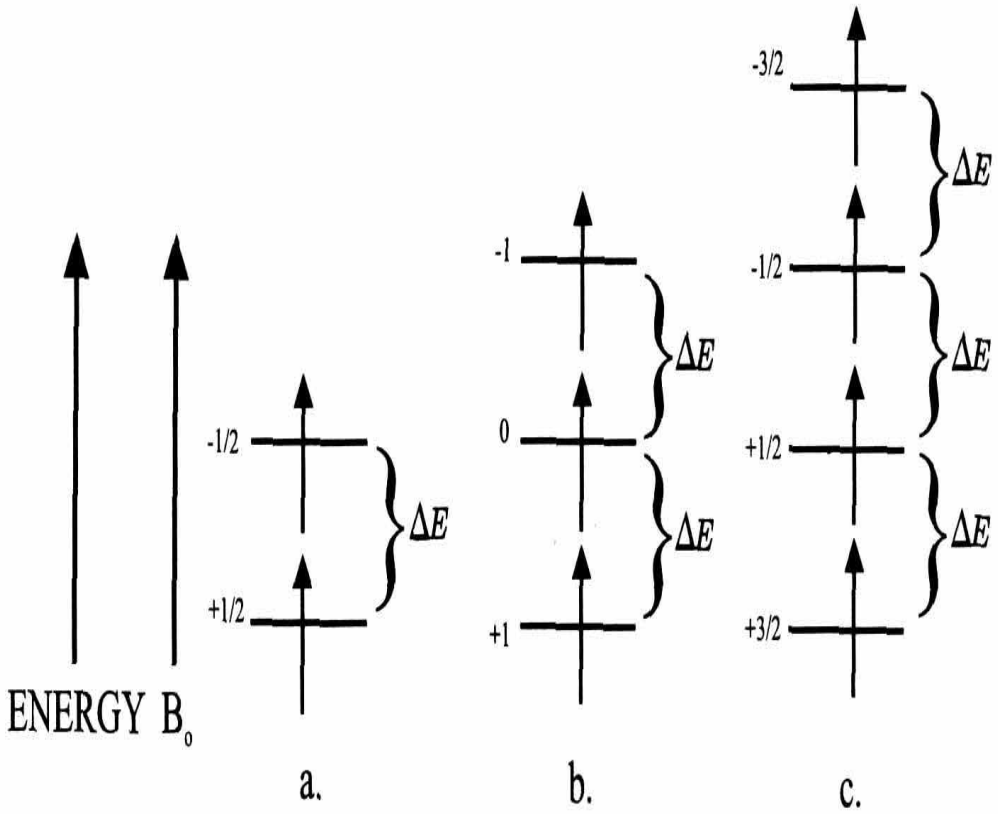

Figure 2.6. Zeeman interaction. In the presence of a magnetic field, the energy states for a spin become unequal. The difference in energy ΔE between any two states is the same and is proportional to B_0. For most spin ½ nuclei, the $z = +½$ level is lowest in energy (*a*); for most spin 1 nuclei, the $z = +1$ level is lowest in energy (*b*); for most spin ³⁄₂ nuclei, the $z = +³⁄₂$ level is lowest in energy (*c*).

Resonance (共振)

Larmor precession 之角速度

$\omega_0 = \gamma B_0$ ， 故 $\omega_0 = 2\pi\nu$

亦即， 如果我們介入一固定頻率 ν ，便可準確的協調 **Larmor** 旋轉的頻率 。也就是說，介入的頻率與 **Larmor** 旋轉的頻率發生共振 。

(c) Pulsed NMR and Fourier transform

Pulse NMR against CW NMR

- In the CW experiment, requiring 1 Hz resolution over a 1000 Hz spectral width led to a 1000 s experiment time. Supposing it proves possible to analyze the response of the sample to an impulse instead, we can evidently complete this alternative experiment in just 1 s, because while the requirement for spending 1 s on the measurement of each frequency remains, we are measuring all frequencies simultaneously instead of one after another.

Fourier transform

- The Fourier transform allows us to interconvert the amplitude evolving in the time domain into the frequency domain :
- $f(\omega) = \int f(t) \exp(i\omega t)\, dt$
- The integral can be approximated as a sum of signals at different frequencies.

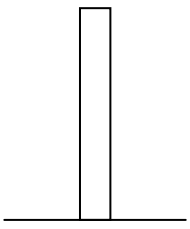

$\equiv \Sigma_n A_n \exp(-i\omega_n t)$

A pulse can be expanded in terms of infinite plane waves

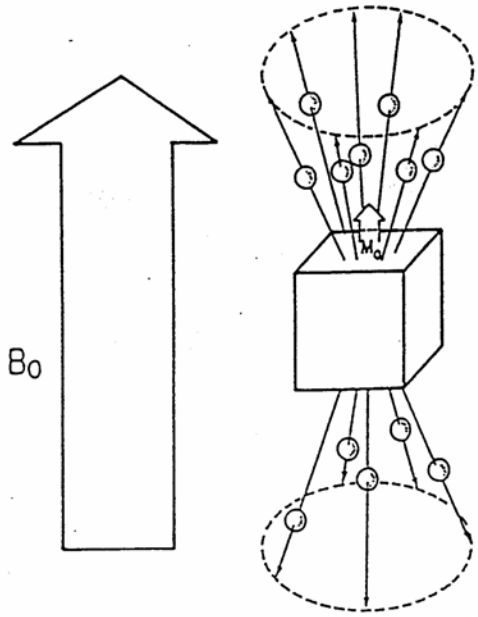

Figure 5. The net magnetization (M_0) resulting from the imbalance of hydrogen nuclear dipoles points along B_0 but is small compared with B_0.

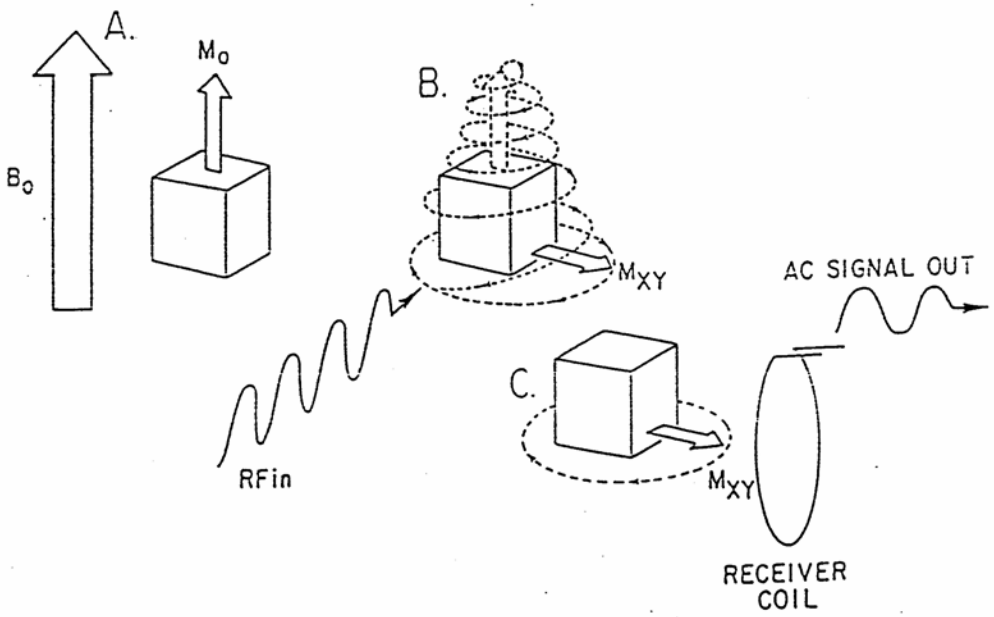

Figure 6. *A.* Net magnetization of the sample M_0 initially is aligned with the main magnetic field B_0, but it is so small in comparison to B_0 that it is undetectable. *B.* A radio-frequency (RF) field applied at the Larmor frequency tips tissue magnetization into the transverse plane, rendering it measurable as transverse magnetization, M_{xy}. *C.* Measurement of M_{xy} is possible because of its precession, which produces a changing magnetic flux linking a properly oriented loop receiver coil. The changing magnetic flux linking the coil induces an alternating current (AC) (alternating at the Larmor frequency) in the receiver coil. This alternating current, when amplified and digitized, becomes the signal from which the MR image is reconstructed.

3D-FID (Free Induction Decay)

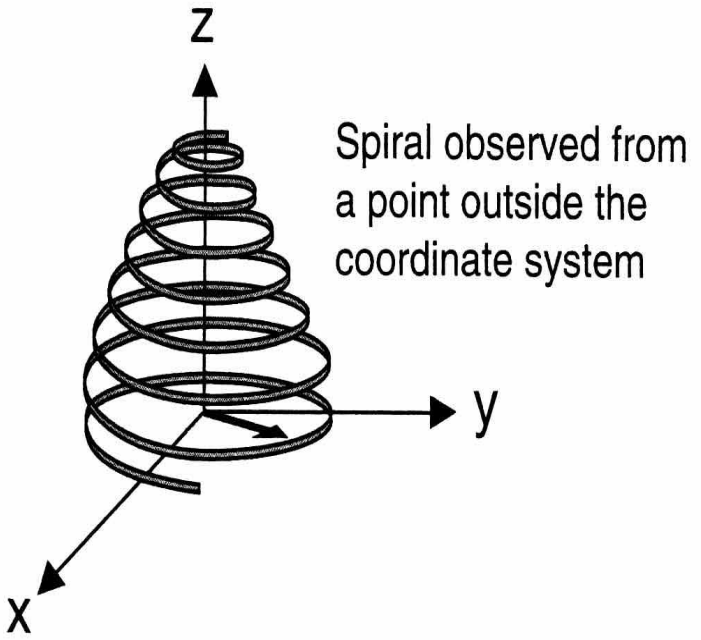

The outside observer sees a spiral motion of the magnetization vector towards the x-y plane.

共振後磁向量的軌跡

Fourier Transform

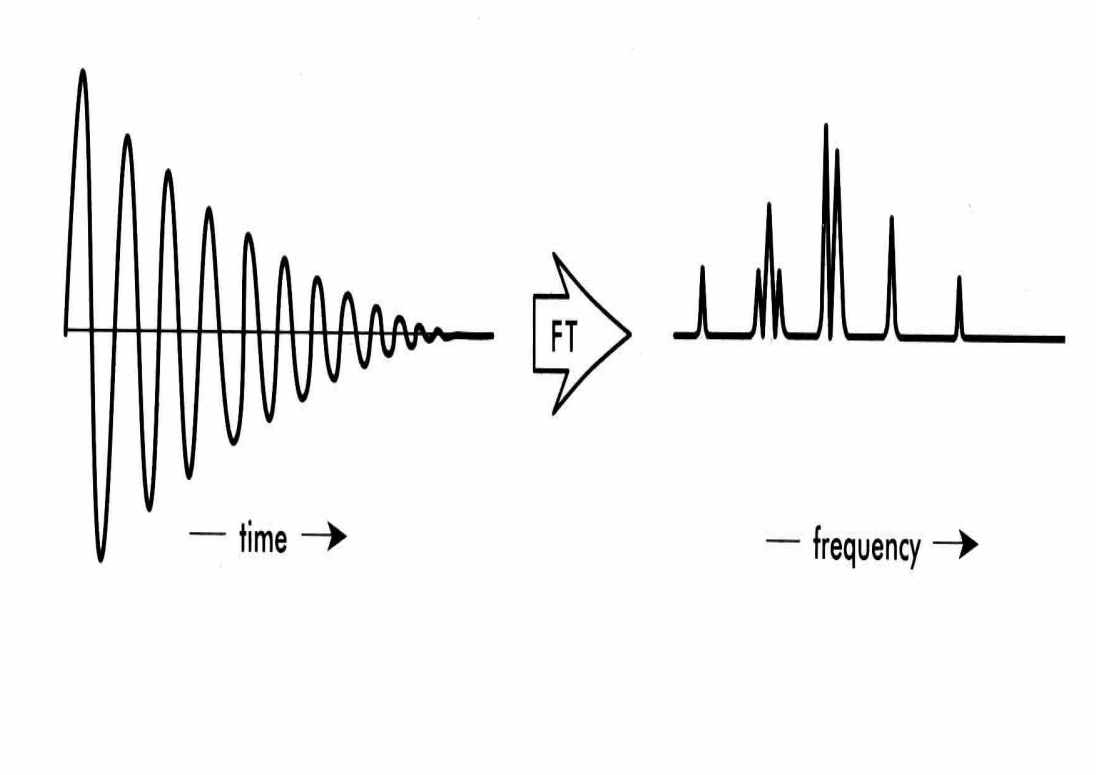

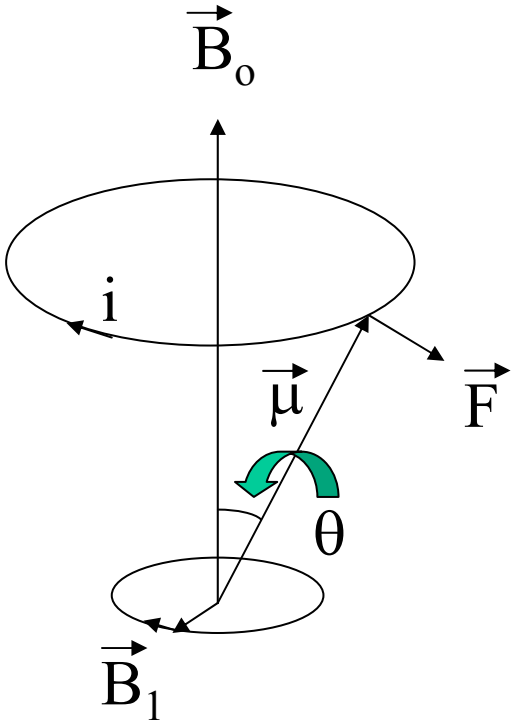

Suppose there is an additional weak magnetic field, B_1, perpendicular to B_o. Such a field will also exert a torque on μ, tending to change the angle θ between μ and B_o. However, if B_1 is fixed in direction it will alternately try to increase and decrease θ as μ precesses. Since B_1 is stated to be weak, the net effect will be a slight wobbling in the precession of μ; such an effect is referred to as nutation. Alternatively, the motion of μ can be described as caused by a resultant field $B_o + B_1$. If, on the other hand, B_1 is not fixed in direction, but is rotating about B_o with the same frequency as the precession of μ and in the same direction, its orientation with respect to μ will be constant. Suppose this orientation is such that B_1 is always perpendicular to the plane containing B_o and μ, then the torque exerted on μ by B_1 will always be away from B_o. Consequently, a large effect on μ is possible. Since changing θ corresponds to changing the energy of μ in B_o, this condition is described as resonance-the frequency, υ, of the field B_1 required must equal the Larmor precession frequency.

Detection and Acquisition

- Consider a proton spectrum recorded at 500 MHz. The various rf signals arising from the sample are all in the region of 500 MHz, differing only by the chemical shift range present. For protons this would typically be 10 ppm or 5000 Hz, so the frequencies encountered might run from 500,000,000 Hz to 500,005,000 Hz. There is no objection in principle to attempting direct digitization of these signals. We are left only with the chemical shifts to digitize, in this case frequencies from 0 to 5000 Hz.

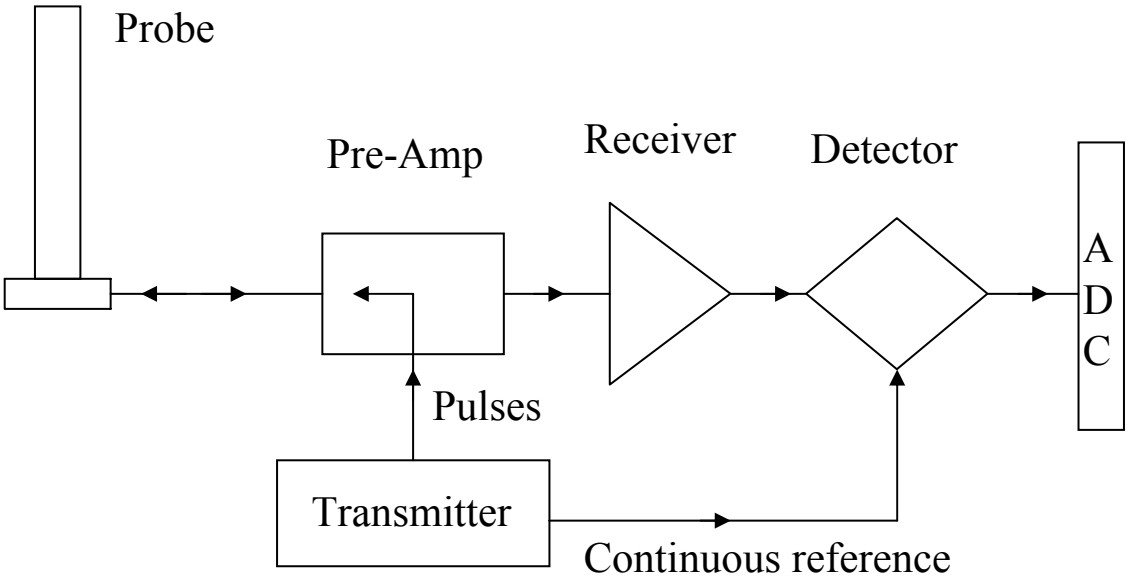

(d) Chemical shifts

The magnetic shielding and chemical shift

Consider an indirect coupling of the nuclei to external static magnetic field by interacting with the surrounding electrons. This interaction leads to magnetic shielding in resonance frequencies that are a reflection of the chemical environment of a nucleus in an atom or molecule and are therefore important in the analytical application of NMR, as well as in testing theoretical descriptions of molecules.

B=Bo(1-σ), The dimensionless number σ is a small fraction, describing the electron shielding in the external magnetic field.

NMR parameters

Chemical shift (δ) ***defines the location of a NMR line along the rf axis. It is measured relative to a reference compound. In frequency units the chemical shift is proportional to the applied static magnetic field, and therefore chemical shifts are customarily quoted in parts per million (ppm) units.***

$$\Delta\nu = \nu_{\text{signal}} - \nu_{\text{reference}}$$

$$\delta\ (\text{ppm}) = (\Delta\nu/\nu_0) \times 10^6$$

Nuclear spin (I) :

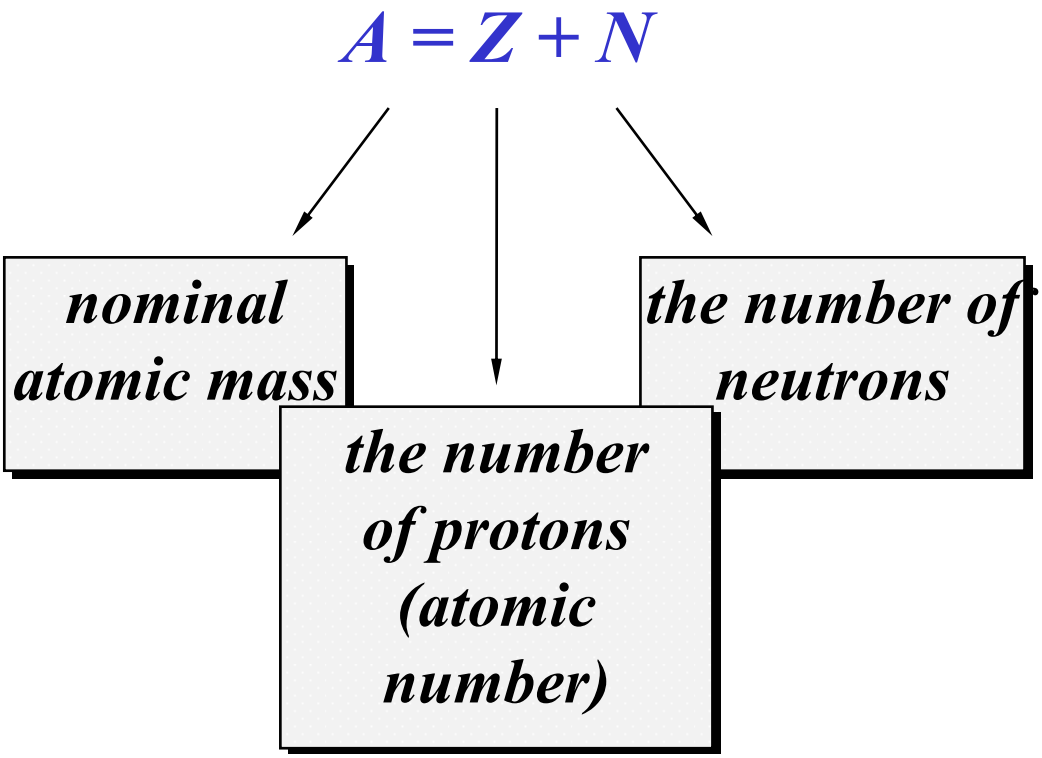

Chemical Shielding

Consider an indirect coupling of the nuclei to external static magnetic field by interaction with the surrounding electrons. This interaction leads to shifts in resonance frequencies that are a reflection of the chemical environment of a nucleus in an atom or molecule and are therefore important in the analytical application of NMR, as well as in testing theoretical descriptions of molecules.

Anisotropic Interaction
Solid State NMR Spectroscopy

- *C*hemical *S*hift *A*nisotropy (CSA)
  ^{1}H, ^{13}C, ^{19}F (~5kHz, 10~100 kHz, ~100 kHz)

- Dipolar interaction
  homonuclear : ^{1}H-^{1}H, ^{13}C-^{13}C, ^{19}F-^{19}F; ~50 kHz, 2 kHz, ~32 kHz

  heteronuclear : ^{1}H-^{13}C, ^{1}H- ^{19}F, ^{19}F- ^{13}C; ^{15}N-^{13}C;
  25 kHz, 35 kHz, 10 kHz, 800~200 Hz

- Quadrupolar interaction, I > 1/2 ^{2}H ~ 40 kHz

  resulting in information about
  molecular structure
  molecular dynamics
  (cover a wide range of 10^{-10} ~ 10^{+3}s)
  orientational order
  morphology, conformation
  mobility

* Both CSA and Quadrupolar interactions are external magnetic field dependent.

How to average the anisotropic interaction ?

Solid State NMR Spectroscopy

Line-narrowing factors

Intrinsic molecular motions – close to the "size" of anisotropic interactions

MAS(*M*agic *A*ngle *S*pinning) sample spinning, rotation axis exactly tilted by 54.7^{o} away from static magnetic field direction

Multiple-pulse technique; explained by average Hamiltonian theory (AHT)

*CP and MAS are commonly used methods in solid-state NMR

How to enhancee the NMR signal of rare spin ?

1D CP/MAS (cross-polarization/magic angle spinning) technique

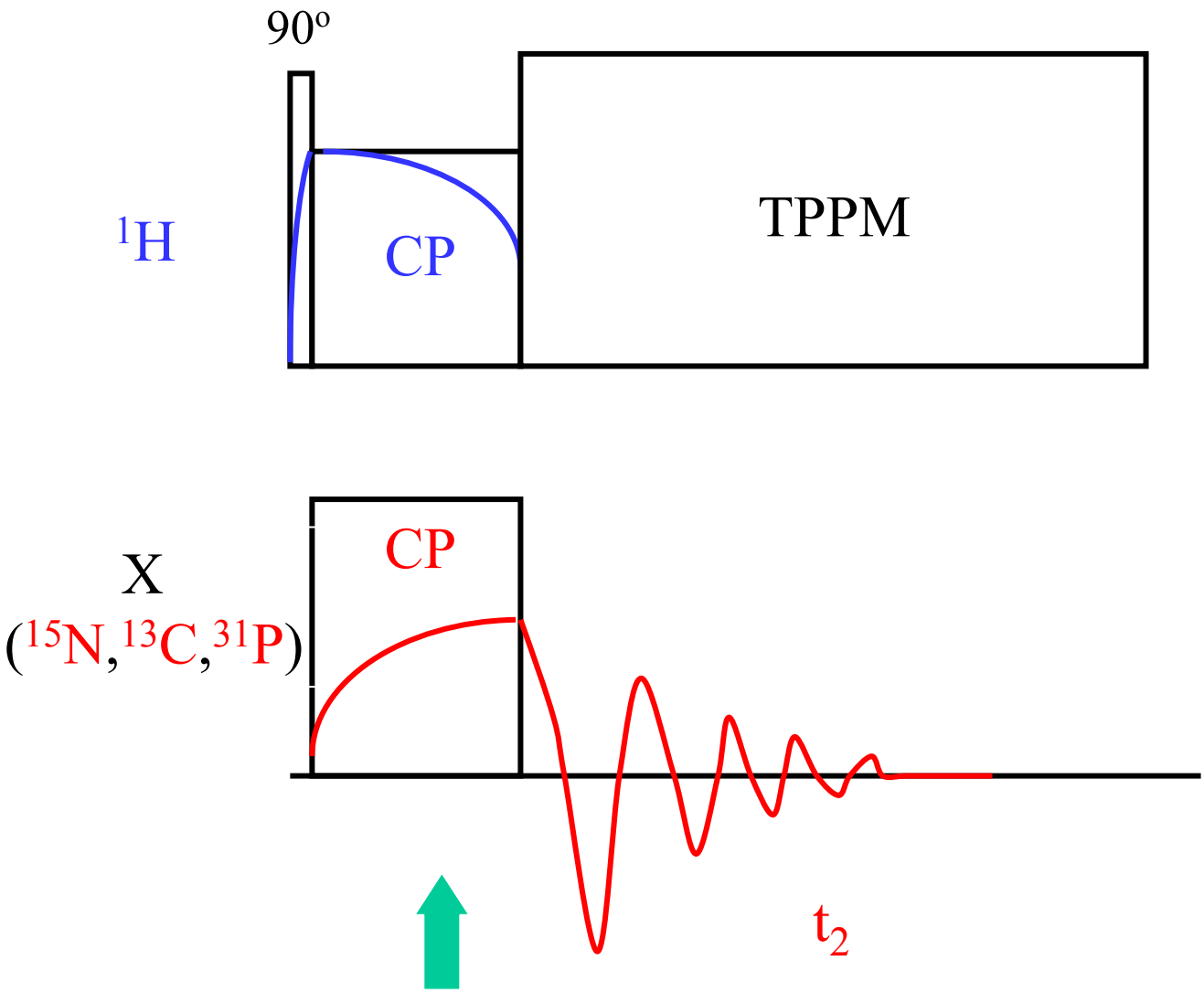

Hartmann Hahn condition :

$B_{1H}\gamma_H = B_{1X}\gamma_X$

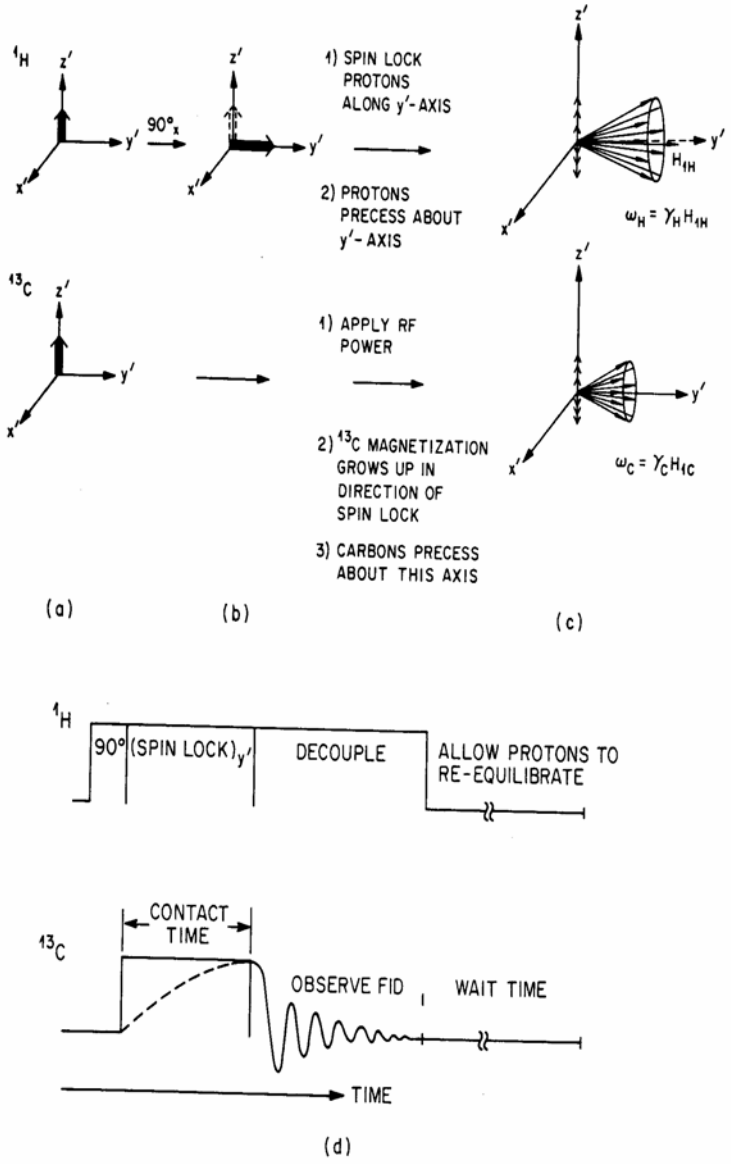

Figure 3.8 ■ (a), (b), and (c) are vector diagrams for a ^{1}H and ^{13}C double rotating-frame CP experiment. (d) gives the CP pulse sequence. [Reprinted with permission from Jelinski (1982).]

TABLE 2

Typical Magnitudes and Orientations of Chemical Shift, Scalar *J* Coupling, Dipole–Dipole Coupling, and Quadrupolar Coupling Tensors within the Amino Acid Residue or Peptide Plane of Polypeptides[a]

Chemical shift	Spin	δ_{iso}^{CS}	δ_{aniso}^{CS}	η^{CS}	α_{PE}^{CS}	β_{PE}^{CS}	γ_{PE}^{CS}	Ref.
	$^{1}H^{N}$	9.3	7.7	0.65	90	−90	90	*31*
	$^{13}C^{\alpha}$[b]	50	−20	0.43	90	90	0	*32, 33*
	$^{13}C'$	170	−76	0.90	0	0	94	*34–36*
	^{15}N	119	99	0.19	−90	−90	−17	*31, 35–37*
J and dipolar coupling	Spins	J_{iso}^{IS}[c]	$b_{IS}/2\pi$[d]	r_{IS}^{e}	β_{PE}^{D}	γ_{PE}^{D}		
	$^{1}H^{\alpha}$–$^{13}C^{\alpha}$	140	−23328	1.090	—[f]	—[f]		
	$^{1}H^{N}$–^{15}N	−92	11341[g]	1.024[g]	90	0		
	$^{13}C^{\alpha}$–$^{13}C'$	55	−2142	1.525	90	120.8		
	$^{13}C^{\alpha}$–$^{13}C^{\beta}$	35	−2159	1.521	—[f]	—[f]		
	$^{13}C^{\alpha}$–^{15}N	−11	988	1.458	90	115.3		
	$^{13}C'$–^{15}N	−15	1305	1.329	90	57		
Quadrupolar coupling	Spin		C_Q	η^{Q}	α_{PE}^{Q}	β_{PE}^{Q}	γ_{PE}^{Q}	Ref.
	$^{2}H^{N}$[h]		0.210	0.15	−90	90	0	*38*
	$^{2}H^{\alpha}$		0.168	0.10	—[f]	—[f]	—[f]	*39, 40*
	^{14}N		3.21	0.32	0	0	0	*35, 41*
	^{17}O[h,i]		8.3	0.28	−90	90	0	*42*

[a] The Euler angles relate the principal axes frames (P^{λ}) to the peptide plane (E) having x_E along N–H and z_E being the normal to the plane (cf. Fig. 2a). Chemical shifts (δ_{iso}^{CS}, δ_{aniso}^{CS}; defined in Ref. *17*) are in ppm relative to TMS (^{1}H, ^{13}C) and liq. NH_3 (^{15}N). Scalar *J* and dipolar couplings (J_{iso}^{IS} and $b_{IS}/2\pi$) are given in Hz, the internuclear distance r_{IS} in Å, and the quadrupolar coupling in MHz. Due to axial symmetry the dipolar coupling α_{PE} (and $\alpha_{PC'}$) angle can be chosen arbitrarily.

[b] The orientation of the $^{13}C^{\alpha}$ chemical shielding tensor depends on the secondary structure and may vary significantly from the given angles (*43*).

[c] Scalar coupling constants taken from Ref. (*44*).

[d] Dipole couplings calculated from r_{IS}.

[e] Typical N–H and C–H bond lengths are taken from Ref. (*22*), while N–C and C–C bond lengths are taken from Ref. (*21*). We note that SIMMOL automatically calculates the bond length; dipolar coupling constants, and dipolar coupling Ω_{PC}^{D} Euler angles directly from the PDB structure without reference to the tabelized values.

[f] The Euler angles depend on the secondary structure.

[g] A somewhat lower value of $b_{IS}/2\pi = 9.9$ kHz (corresponding to $r_{IS} = 1.07$ Å) is typically used for peptides oriented in uniaxially aligned phospholipid bilayers (*45*).

[h] We note that the magnitude and in particular the orientation of these tensors may be influenzed by hydrogen bonding.

[i] We assume that the ^{17}O quadrupolar coupling tensor is oriented with its unique element Q_{zz} along the C′–O bond axis and Q_{yy} perpendicular to the peptide plane.

α-^{13}C Chemical Shift Values Categorized According to Secondary Structural Assignment[a-d]

Residue[e] type	Helix (DDS)	β Strand (DDS)	Coil (DDS)	Spera (1991) (TSP)	Richarz (1978) (dioxane)
Ala (112)	54.7	50.3	52.4	52.3	50.8
Cys (27)	60.0	56.1	56.0	56.9	53.9
Asp (97)	56.7	52.3	54.2	54.0	52.7
Glu (132)	59.2	54.6	56.4	56.4	55.4
Phe (74)	60.7	56.1	57.8	58.0	56.2
Gly (121)	46.5	44.6	45.4	45.1	43.9
His (24)	58.5	55.1	55.5	-	53.6
Ile (86)	64.7	59.8	61.3	61.3	59.6
Lys (138)	59.3	54.8	56.6	56.5	54.6
Leu (113)	57.8	53.9	55.7	55.1	53.8
Met (36)	57.8	54.1	55.7	55.3	54.0
Asn (71)	55.8	51.9	55.7	52.8	51.5
Pro (53)	65.9	62.5	53.2	63.1	61.9
Gln (61)	58.7	54.0	55.8	56.1	54.1
Arg (65)	59.4	54.8	56.7	56.1	54.6
Ser (88)	61.2	56.8	58.2	58.2	56.6
Thr (105)	65.8	60.6	62.0	62.1	60.1
Val (114)	65.7	60.0	62.3	62.3	60.7
Trp (12)	59.0	55.2	56.4	57.7	55.7
Tyr (43)	60.7	56.6	57.5	58.1	56.3

[a] Experimentally measured random coil values from Richarz and Wuthrich and from Spear and Bax are included for comparison. Data are given in ppm.

[b] The compounds (DDS, TMS, or dioxane) used in referencing the data are shown at the top of each column.

[c] To adjust DSS values to "old" dioxane standard, substract 1.5 ppm.

[d] To adjust DSS values to TSP, add 0.1 ppm.

[e] Total number of residues observed is given in parentheses. The data cover a grand total of 1572 amino acids.

Random Coil Chemical Shifts for Backbone Atoms in Peptides and Proteins[a]

Residue	α-^{1}H[b]	N-^{1}H	2-^{13}C	1-^{13}C	^{15}N
Ala	4.33	8.15	52.2	177.6	122.5
Cys	4.54	8.23	56.8	174.6	118.0
Asp	4.71	8.37	53.9	176.8	120.6
Glu	4.33	8.36	56.3	176.6	121.3
Phe	4.63	8.30	57.9	175.9	120.9
Gly	3.96	8.29	45.0	173.6	108.9
His	4.60	8.28	55.5	174.9	119.1
Ile	4.17	8.21	61.2	176.5	123.2
Lys	4.33	8.25	56.4	176.5	121.5
Leu	4.32	8.23	55.0	176.9	121.8
Met	4.48	8.29	55.2	176.3	120.5
Asn	4.74	8.38	52.7	175.6	119.5
Pro	4.42	-	63.0	176.0	128.1
Gln	4.33	8.27	56.0	175.6	120.3
Arg	4.35	8.27	56.0	176.6	120.8
Ser	4.47	8.31	58.1	174.4	116.7
Thr	4.35	8.24	62.0	174.8	114.2
Val	4.12	8.19	62.2	176.0	121.1
Trp	4.66	8.18	57.6	173.6	120.5
Tyr	4.55	8.28	58.0	175.9	122.0

[a] Proton and carbon shifts are relative to DDS, nitrogen shifts are relative to NH_3. Data are given in ppm.

[b] α-^{1}H shifts were measured using the hexapeptide GGXAGG in 1M urea at 25C.

Wishart and Skyes, Methods Enzymol. (1994), **239** ,363-392.

(a) Chemical Shift Anisotropy

It has been assumed that, provided that dipole interactions could be removed, solid state NMR spectra would be entirely analogous in appearance with those of the solution state. This not the case because of a facet of shielding not hitherto considered in any detail, namely that shielding constants depend on the orientation of the nuclear environment in the applied magnetic field.

A nuclear environment with less symmetry will have its shielding characterized by *three* unique values. This is typical of a *tensor* property, for which the three values are referred to as the principal components and occur for orientations specified by the principal axes in a molecule-fixed system.

In the general case the observed shielding constant is denoted σ_{obs} and is a linear combination of the principal component, σ_{ii};

$$\sigma_{obs} = \Sigma\, \sigma_{ii} \cos^2\theta_{ii} \ ;$$

θ_{ii} are the angles between the σ_{ii} and B_o.

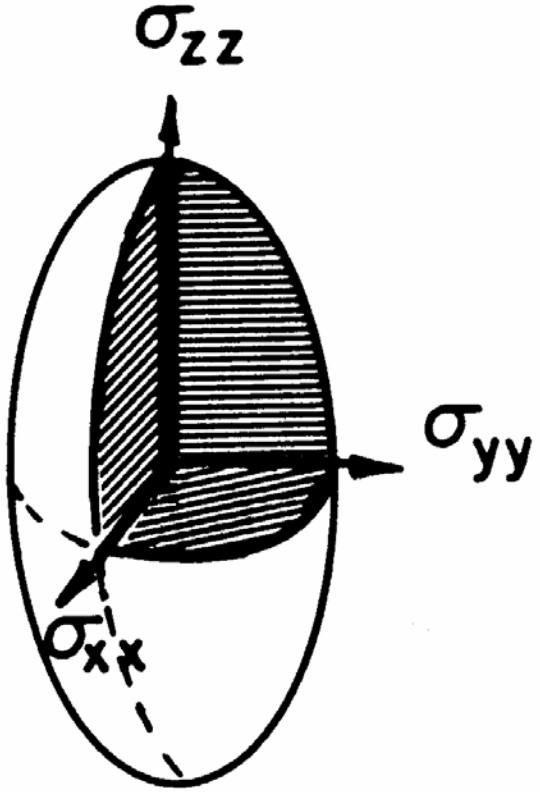

FIG. 3.5. The chemical shielding ellipsoid, which is used to indicate that different orientations of the magnetic field relative to the molecular framework result in different resonance positions for the same chemical species.

Chemical Shift Anisotropy

The resonance frequency Ω is orientation dependent, in the first order perturbation theory one obtains,

$$\sigma = \sigma_0 + \frac{1}{2}\Delta(3Cos^2\vartheta - 1 - \eta Sin^2\vartheta Cos^2\varphi)$$

σ_0 : isotropic chemical shift;
$\sigma_{iso} = (\sigma_{11} + \sigma_{22} + \sigma_{33}) / 3$

$\Delta = (\sigma_{33} - \sigma_{iso})$, describes the strength of the anisotropic coupling, or ^{13}C–^{1}H dipole-dipole coupling for ^{13}C or quadrupole coupling for ^{2}H

$\eta = \frac{\sigma_{22} - \sigma_{11}}{\sigma_{33} - \sigma_{iso}}$; $(0 \leq \eta \leq 1)$ asymmetry parameter representing the deviation of the anisotropic coupling from axial symmetry

ϑ, φ : polar angles of the magnetic field B_0 in the principal axes system of the coupling tensor

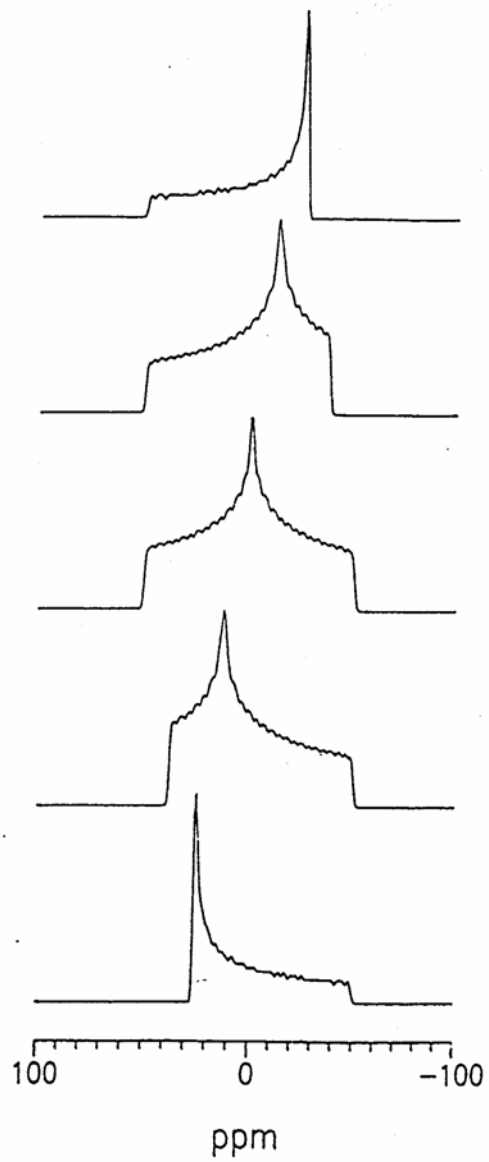

FIGURE 12 Computer-simulated NMR lineshapes due to chemical shift interactions at different η_{cs} values. The chemical shift parameters used are, from top to bottom, -25, -25, and 50; -37.5, -12.5, and 50; 50, 0, and -50; 12.5, 37.5, and -50; 25, 25, and -50, respectively.

Static Sample

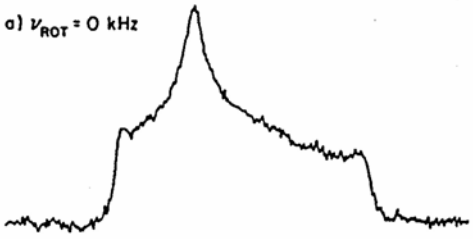

MAS (*M*agic *A*ngle *S*pinning)

Lab. Frame

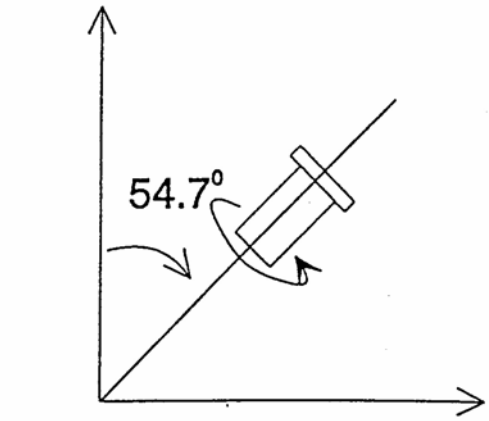

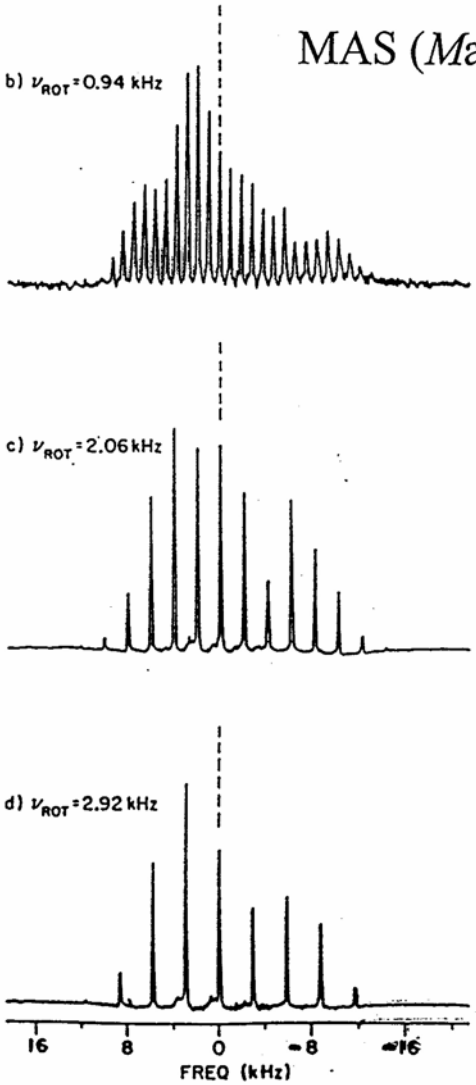

Fig. 2.12. Proton decoupled ^{31}P sideband spectra (119.05 MHz) of solid dipalmitoyl phosphatidylcholine spinning at the magic angle according to R.G. Griffin, published in [9]. ν_{Rot} indicates the spinning frequency

Reconstruction of CSA tensor

- Based on the MAS sidebands one can reconstruct the CSA tensor principal values
- The degree of the accuracy relies on the number of the spinning sideband the more spinning sideband the higher degree of accuracy. Generally, it is expected to have accurate measurement for nuclei that have a large shielding anisotropy.
- Herzfeld and Herger's analysis

  (J. Chem. Phys., 73, 6021-6030 (1980).

1D ^{13}C CP/MAS spectra of $^{13}C_1$-labeled GlcN acquired at indicated MAS speed.

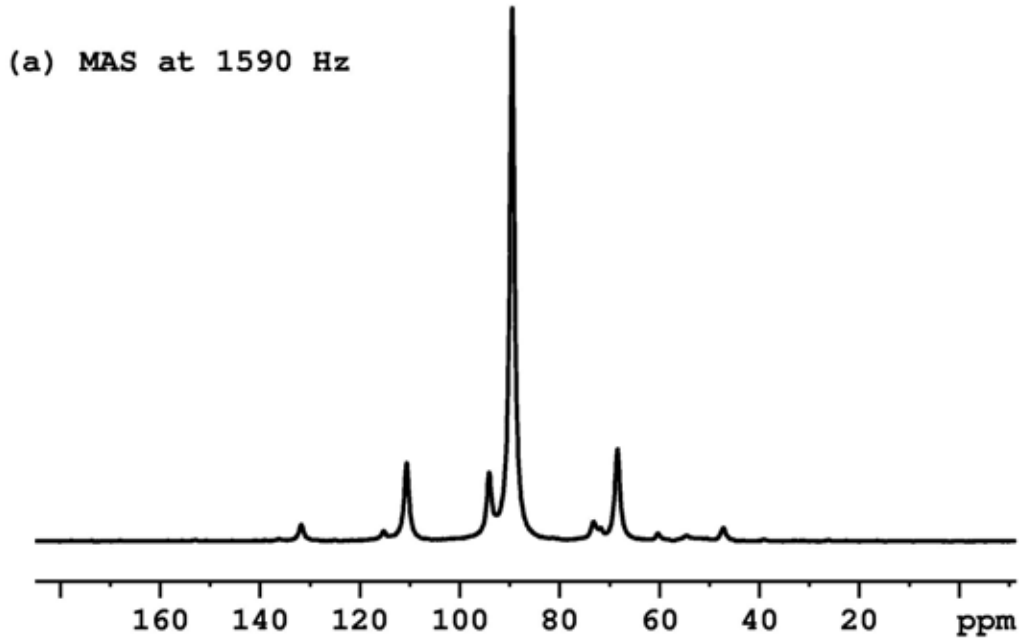

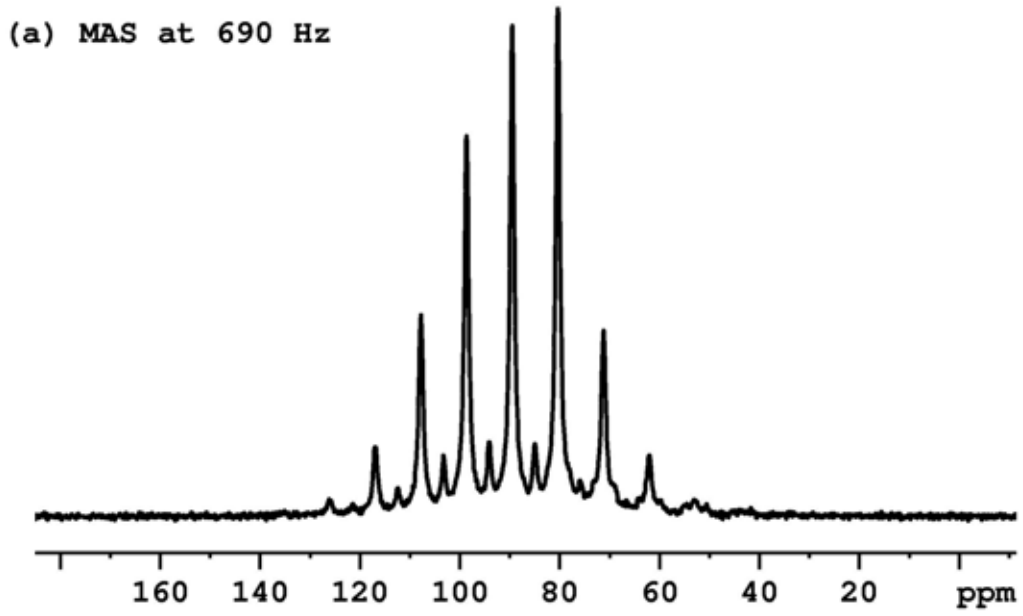

Table 1. Summary of ^{13}C chemical shifts, chemical shift tensor elements, dipolar strengths, and free-energy differences for the anomeric α and β forms in Glc, Man, Gal, GalN, GlcN, and GlcNAc[a]

	Glc		Man		Gal		GalN		GlcN		GlcNAc	
	α	β	α	β	α	β	α	β	α	β	α	β
Relative population %[b]	82 (48)	18 (48)	48 (51)	52 (48)	96 (48)	4 (33)	98 (44)	2 (49)	90 (58)	10 (76)	80 (73)	20 (98)
σ_{iso}[c]	93.4	97.0	91.2	94.7	92.4	96.7	89.7	95.1	89.3	93.9	93.0	96.8
σ_{33}	66.9	70.2	67.1	74.7	65.8	71.3[d]	61.4	68.0[d]	62.4	68.8	67.0	73.7
σ_{22}	97.3	99.2	98.7	99.8	95.2	96.0[d]	96.4	99.3[d]	92.0	95.8	97.7	99.8
σ_{11}	115.9	121.6	107.9	110.0	116.2	115.8[d]	111.4	111.7[d]	113.4	117.1	114.3	117.0
$-(\sigma_{33} - \sigma_{iso})$	26.5	26.8	24.1	20.1	26.6	25.4	28.3	27.1	26.9	25.1	26.0	23.1
η[e]	0.70	0.84	0.38	0.51	0.79	0.78	0.53	0.46	0.80	0.86	0.64	0.74
$\Delta\sigma$[f]	−39.7	−40.2	−36.2	−30.2	−39.9	−34.6	−42.5	−37.5	−40.7	−37.7	−39.0	−34.6
D (Hz)[g]							−200		−200	−200	−180	−180
r (Å)[h]							2.48		2.48	2.48	2.57	2.57
ΔE (kcal/mol)	0.90		−0.05		1.88		2. 30		1.30		0.82	

[a] Samples were specifically ^{13}C- and/or ^{15}N-labeled. For details, see Experimental. Chemical shift tensor elements were the average of measurements at various MAS speeds with standard deviation of ±0.5 ppm.

[b] Data was deduced from Lorentzian curve fitting with an uncertainty of ±3%; the half-width at half-height of the fitting curve are given in bracket in unit of Hz.

[c] Chemical shifts were referenced to the carbonyl carbon of glycine at 176.4 ppm.

[d] Data were calculated from that of the α form assuming that the deviation of chemical shift tensor elements from the isotropic chemical shift for the α and β form were the same as that for methyl α- and β-D-galactopyranoside.[13]

[e] Chemical shift tensor axial asymmetry $\eta = (\sigma_{22} - \sigma_{11})/(\sigma_{33} - \sigma_{iso})$.

[f] Chemical shift anisotropy $\Delta\sigma = \sigma_{33} - (\sigma_{11} + \sigma_{22})/2$.

[g] Dipolar strength D was determined from REDOR spectroscopy using the curve-fitting simulation algorithm[7] with an uncertainty of less than 5%.

[h] r is the internuclear distance for ^{13}C-1–{C-2}–^{15}N derived from dipolar strength D.

1D ^{13}C CP/MAS NMR spectra of $^{13}C_1$-labeled GalN (a), GlcN (b) and GlcNAc (c), respectively.

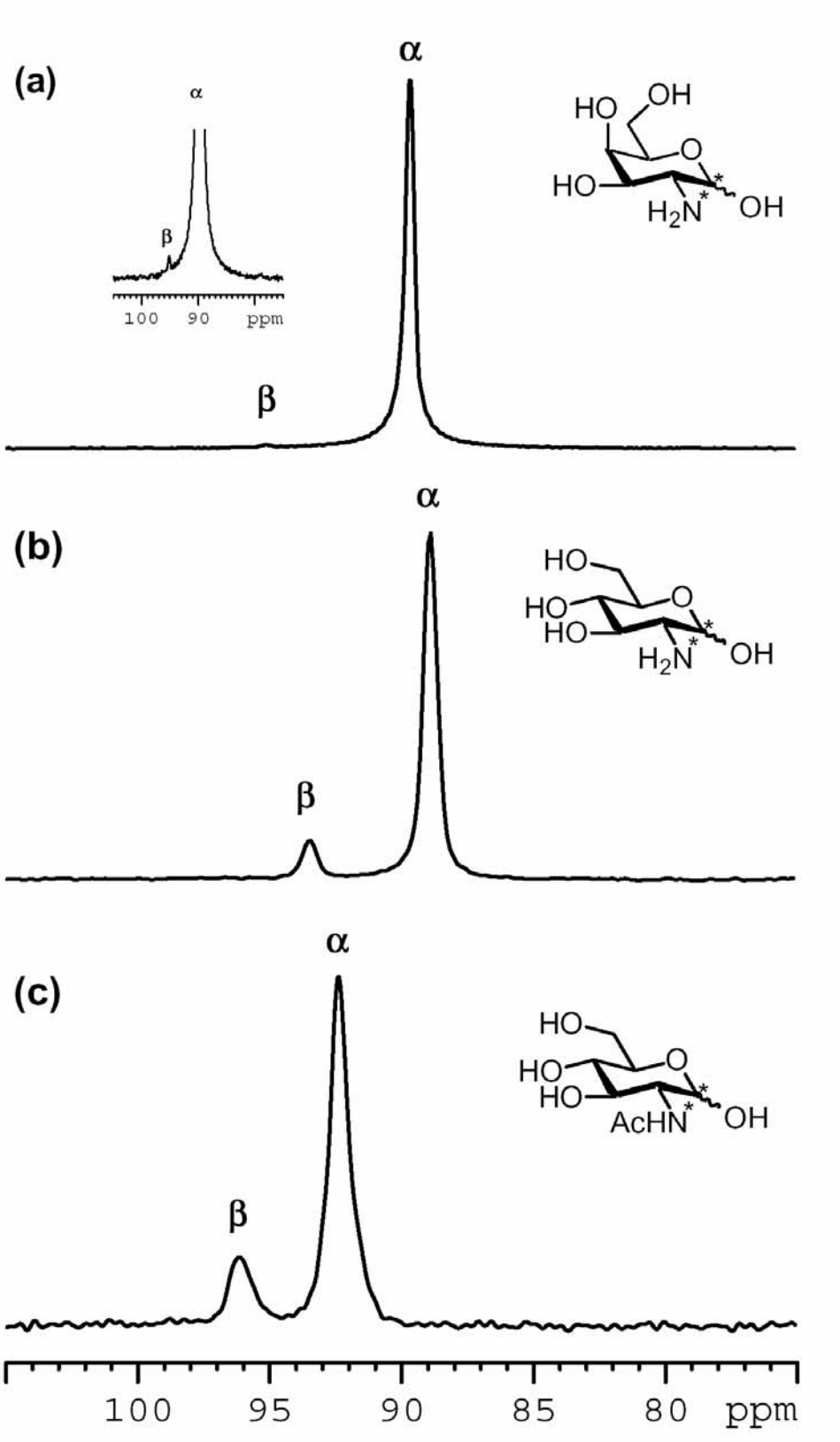

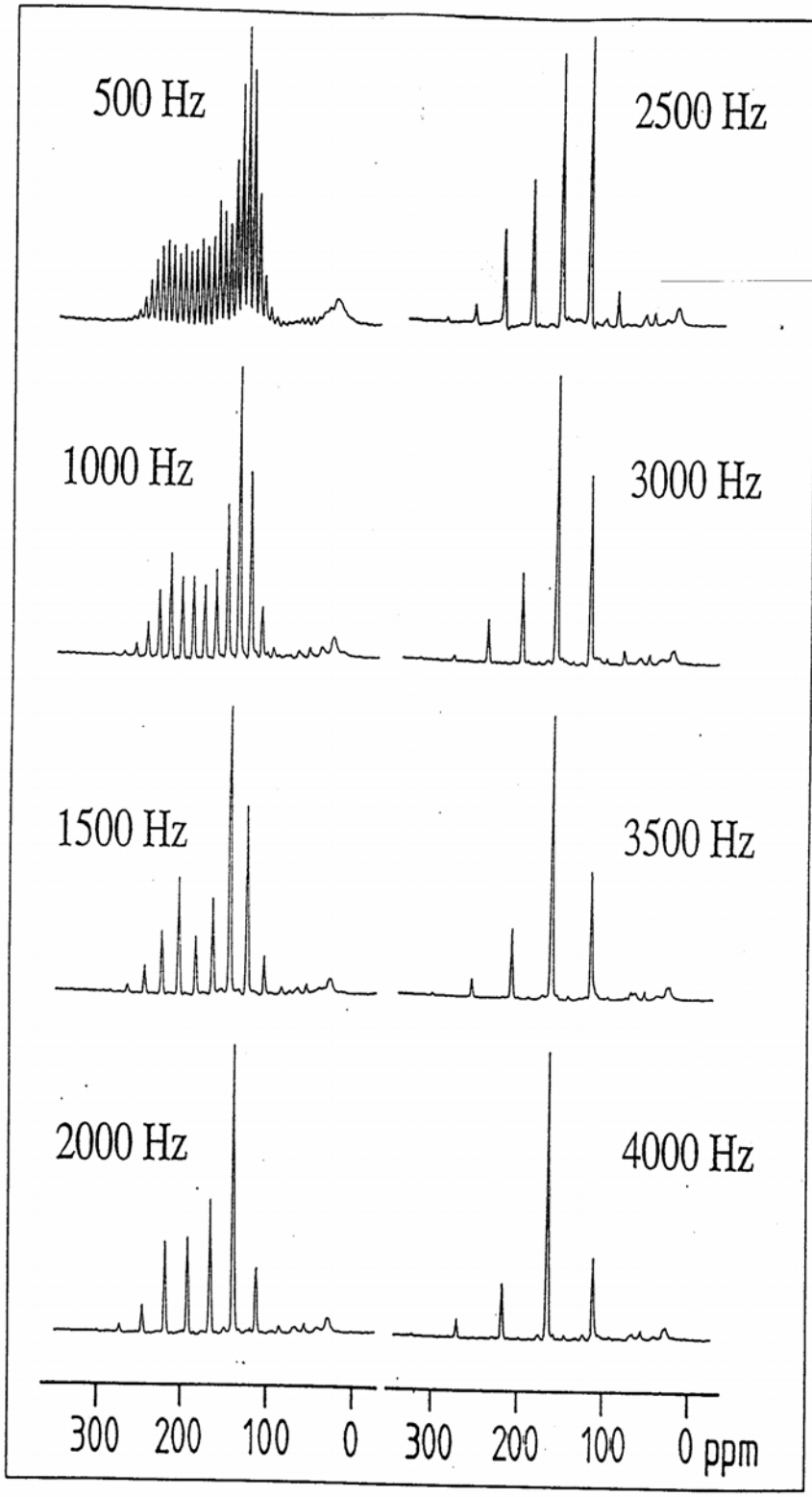

Abb. 3.10. CP-MAS-Spektren von PA6* (Abb. 2.10) bei verschiedenen Rotorfrequenzen. Die im Abstand der Rotorfrequenz auftretenden Seitenbanden enthalten alle Informationen über die Anisotropie der chemischen Verschiebung. Während man für ν_R = 500 Hz noch das zugrundeliegende Pulverspektrum* erkennt, ist das bei ν_R = 4000 Hz nicht mehr der Fall. In natürlicher Häufigkeit vorliegende ^{13}C-Kerne anderer Molekülpositionen führen zu zusätzlichen kleinen Linien.

(b) Dipolar Interaction

Hamiltonian, $\hat{H}$

- The Hamiltonian for a molecule contains terms describing the kinetic energy of each particle, the potential energy of interactions between particles, and interaction of the particles with any external electric or magnetic fields.
- It can be divided approximately into terms representing electronic, vibrational, rotational, and nuclear spin contributions to the energy.
- The nuclear spin states are eigenstates of the Hamiltonian.

Dipolar interaction

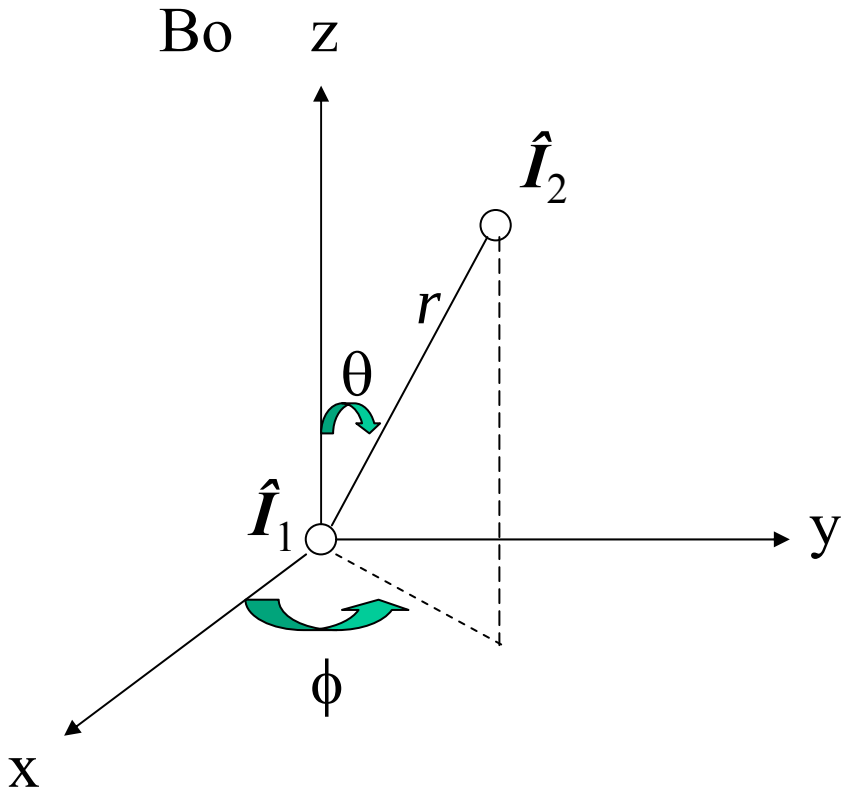

$$\hat{\boldsymbol{I}}_1 = \mathrm{I}_{1\mathrm{x}}\hat{\boldsymbol{e}}_\mathrm{x} + \mathrm{I}_{1\mathrm{y}}\hat{\boldsymbol{e}}_\mathrm{x} + \mathrm{I}_{1\mathrm{z}}\hat{\boldsymbol{e}}_\mathrm{z}$$

$$\boldsymbol{r} = \mathrm{x}\hat{\boldsymbol{e}}_\mathrm{x} + \mathrm{y}\hat{\boldsymbol{e}}_\mathrm{y} + \mathrm{z}\hat{\boldsymbol{e}}_\mathrm{z}$$

Dipolar interaction

- Dipolar Hamiltonian

$$\hat{\boldsymbol{H}} = (\gamma_1\gamma_2\hbar^2\,\mu_o/4\pi)\{I_1\bullet I_2/r^3 - 3(I_1\bullet r)(I_2\bullet r)/r^5\}$$

$$\hat{\boldsymbol{H}} = r^{-3}\,\gamma_1\gamma_2\hbar^2[A+B+C+D+E+F]\,\mu_o/4\pi$$

$$A = -I_{1z}I_{2z}(3\cos^2\theta - 1)$$
$$B = (1/4)[I_{1+}I_{2-}+I_{1-}I_{2+}](3\cos^2\theta - 1)$$
$$C = (-3/2)[I_{1z}I_{2+}+I_{1+}I_{2z}]\sin\theta\cos\theta\exp(-i\phi)$$
$$D = (-3/2)[I_{1z}I_{2-}+I_{1-}I_{2z}]\sin\theta\cos\theta\exp(i\phi)$$
$$E = (-3/4)I_{1+}I_{2+}\sin^2\theta\exp(-2i\phi)$$
$$F = (-3/4)I_{1-}I_{2-}\sin^2\theta\exp(2i\phi)$$

Each of the terms A to F contains a spin factor and a geometrical factor, the effects of which can be appreciated separately. The common factor, $\gamma_1\gamma_2\hbar^2 r^{-3}\,\mu\,o/4\pi$ is sometimes referred to as the dipolar coupling constant. Dipolar coupling is an indirect interaction, being mediated by the electron framework of the molecules

Dipolar Interaction

The dipolar frequency υ

$$\upsilon = \upsilon_o + \frac{1}{2}\Delta(3\cos^2\vartheta - 1)$$

where, $\upsilon_o = (\upsilon_{\parallel} + \upsilon_{\parallel} + \upsilon_{\perp})/3$

$\Delta = (\upsilon_o - \upsilon_{\perp})$, describes ^{13}C–^{1}H dipole-dipole coupling

$$\eta = \frac{\upsilon_{11} - \upsilon_{22}}{\upsilon_{33} - \upsilon_{iso}} = 0;$$

ϑ: is the angle between the magnetic field direction and the dipolar vector.

$$\upsilon = \upsilon_{\parallel}(3\cos^2\vartheta - 1), \text{ where } \upsilon_{\parallel} = \frac{\gamma_I \gamma_S}{r^3}$$

NMR Applications of Dipolar Interaction

(i) Distance information,
sample rotation

(ii) Orientation information
static sample

Rotational-Echo Double-Resonance (REDOR) Spectroscopy

T. Gullion and J. Schaefer, J. Magn. Reson., 81, 196 (1989). T. Gullion and J. Schaefer, Adv. Magn. Reson., Vol. 13, 57 (1989).

Designed to measure weak heteronuclear dipolar coupling of a specific isotope labeled spin pair, for example ^{13}C-^{15}N, even in the presence of large chemical shift anisotropies. Importantly, such measurement can determine accurately internuclear distance between isotope labeled spin pair.

Consider a spin with orientation (α, β) that is initially aligned along the axis in the rf rotating frame. The spin acquired a phase $\phi(\alpha, \beta; t)$ given by

$$\phi(\alpha, \beta; t) = \int_0^{t_1} \omega_D(\alpha, \beta; t)dt$$

$$= \pm \frac{D}{4\omega_r} \left\{ \begin{array}{l} Sin^2\beta[Sin2(\alpha + \omega_r t) - Sin2\alpha] \\ -2\sqrt{2}Sin2\beta[Sin(\alpha + \omega_r t) - Sin\alpha] \end{array} \right\}$$

Average Dipolar Hamiltonian :

In the presence of a single I-spin π pulse, the average precession freq. $\bar{\omega}_D(\alpha, \beta; t)$, which defined over a rotor period.

$$\bar{\omega}_D(\alpha, \beta; t) = \pm \frac{1}{T_r} \int_0^{t_1} \omega_D(\alpha, \beta; t)dt - \int_{t_1}^{T_r} \omega_D(\alpha, \beta; t)dt$$

$$= \pm \frac{D}{4\pi} \left\{ \begin{array}{l} Sin^2\beta[Sin2(\alpha + \omega_r t_1) - Sin2\alpha] \\ -2\sqrt{2}Sin2\beta[Sin(\alpha + \omega_r t_1) - Sin\alpha] \end{array} \right\}$$

The phase accumulation $\Delta\Phi(\alpha, \beta; t)$ of an S spin at the end of the rotor period is

$$\Delta\Phi(\alpha, \beta; t) = \bar{\omega}_D(\alpha, \beta; t)T_r$$

Dipolar orientation in rotating frame

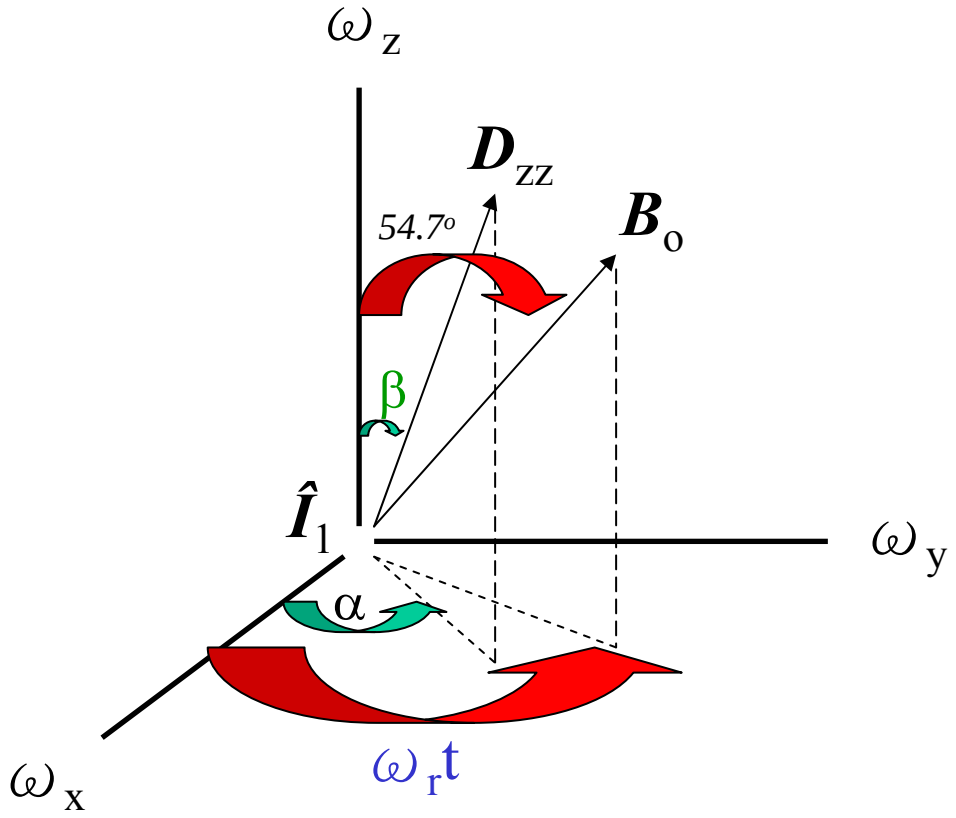

Polar angle: β

Azimuthal angle: $\alpha+\omega_r t$

The specific forms for dipolar and axially symmetric chemical shift interactions are then

$$g_1(t_1) = \cos\left(\frac{\kappa\gamma_I\gamma_S\hbar}{2\omega_r r_{IS}^3}\left\{\frac{\sin^2\beta}{2}[\sin 2(\alpha+\omega_r t_1) - \sin 2\alpha]\right.\right.$$
$$\left.\left. -\sqrt{2}\sin 2\beta[\sin(\alpha+\omega_r t_1) - \sin\alpha]\right\}\right), \qquad (16a)$$

and

$$g_2(t_2) = \exp\left(i\frac{\sigma_{\parallel}}{2\omega_r}\left\{\frac{\sin^2\beta}{2}[\sin 2(\alpha+\omega_r t_2) - \sin 2\alpha]\right.\right.$$
$$\left.\left. -\sqrt{2}\sin 2\beta[\sin(\alpha+\omega_r t_2) - \sin\alpha]\right\}\right). \qquad (16b)$$

M. G. Munowitz and R. G. Grinffin, J. Chem. Phys., 76, 2848-2858 (1982).

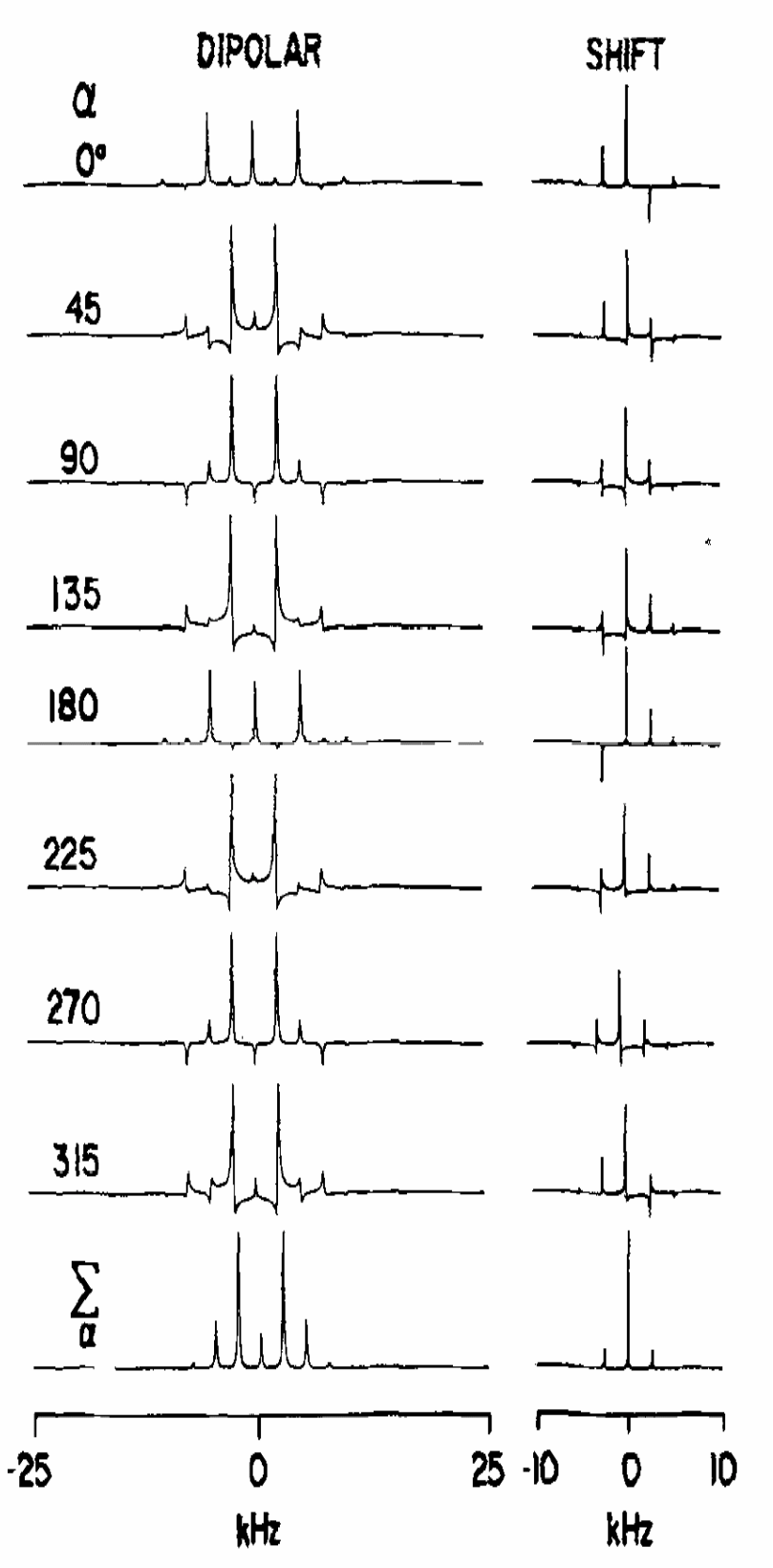

M. G. Munowitz and R. G. Grinffin, J. Chem. Phys., 76, 2848-2858 (1982).

For a power sample, the signal intensity, S(t), at the end of a rotor cycle with one I-spin π pulse is

$$S(t) = \frac{1}{2\pi} \int_{\beta} \int_{\alpha} d\alpha Cos[\Delta\Phi(\alpha, \beta; t)] Sin\beta d\beta$$

In the absence of π pulses on the I channel is

$$S_0 = \frac{1}{2\pi} \int_{\beta} \int_{\alpha} d\alpha Sin\beta d\beta$$

A useful measure of the loss in signal amplitude is the ratio of the difference signal to the full rotatioal-echo amplitude,

$$\Delta S(t)/S_0 = [S_0 - S(t)]/S_0$$

* Which has a strong dependence on the ratio of the dipolar coupling to the spinning speed.

$^{13}C/^{15}N$ Rotational-Echo DOuble-Resonance (REDOR) Spectroscopy

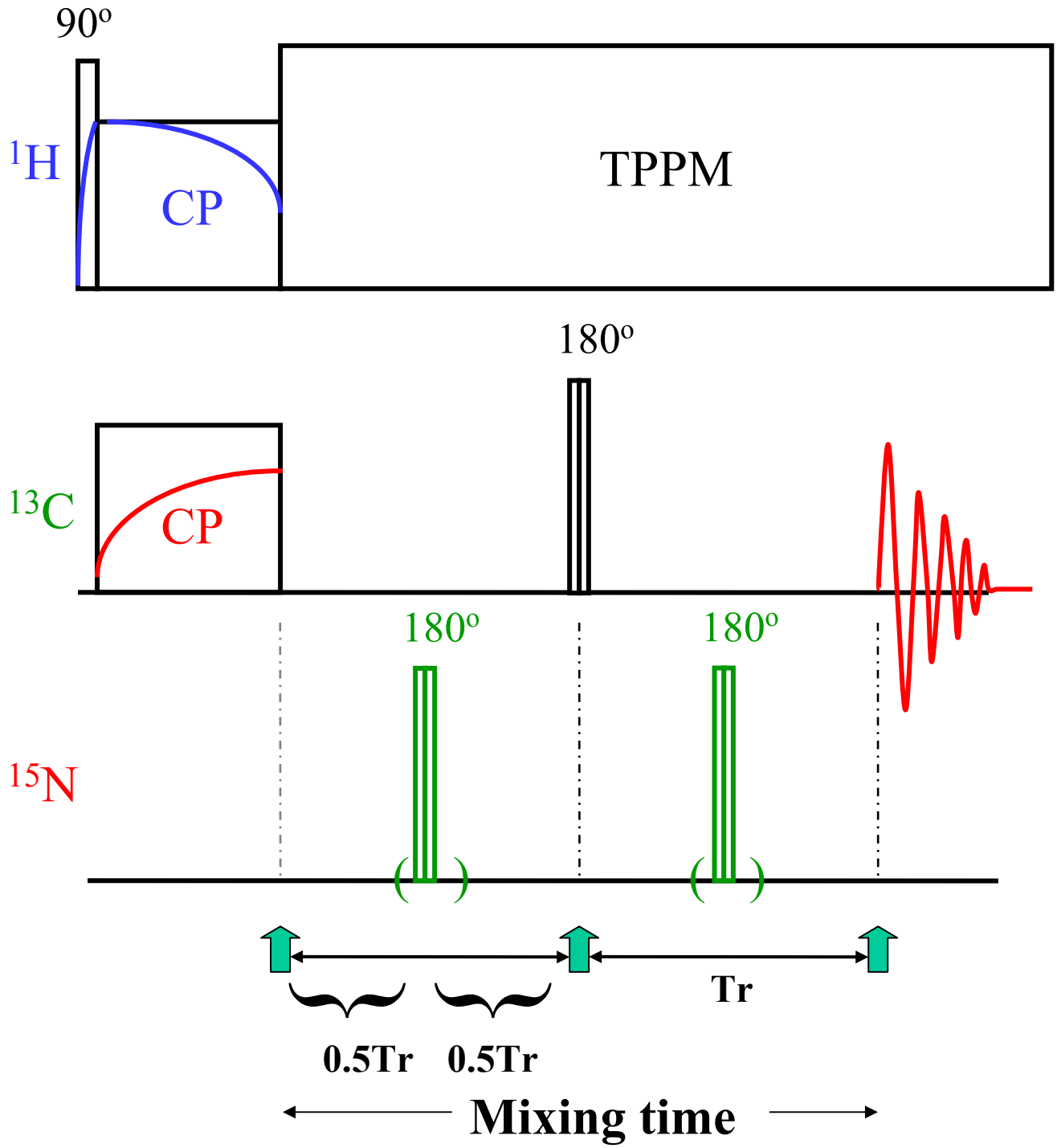

REDOR dipolar dephase curve of $^{13}C/^{15}N$ isotope labeled standard compound Glycine

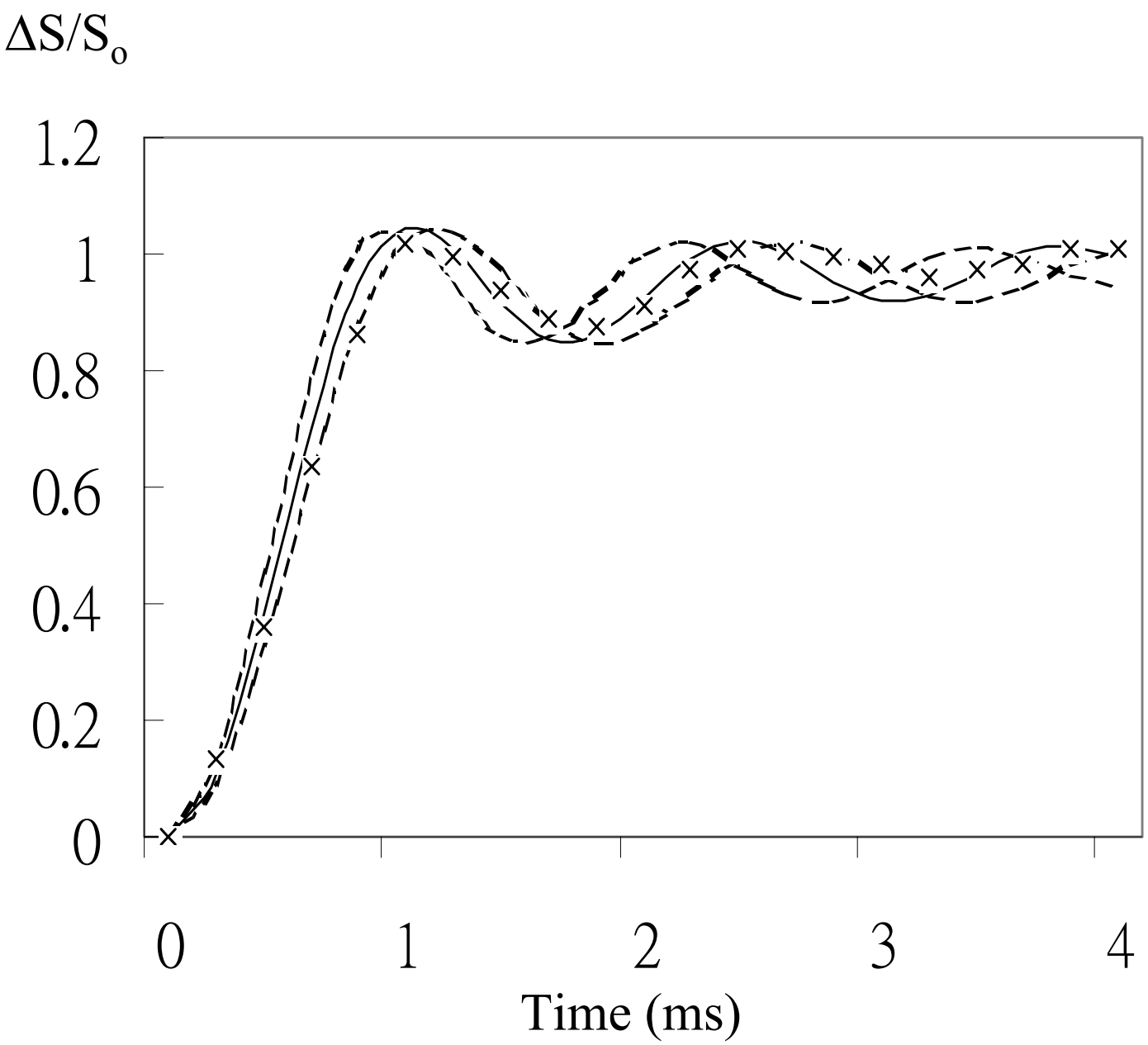

REDOR experiment with an uncertainty of $\pm$0.05 A is demonstrated by glycine dipolar relaxation curve; the solid line D=810 Hz, r=1.554 A, two dot lines D=742, 900 Hz, r=1.6, 1.5 A. and the "x" the experimental data acquired at MAS speed of 5000 Hz.

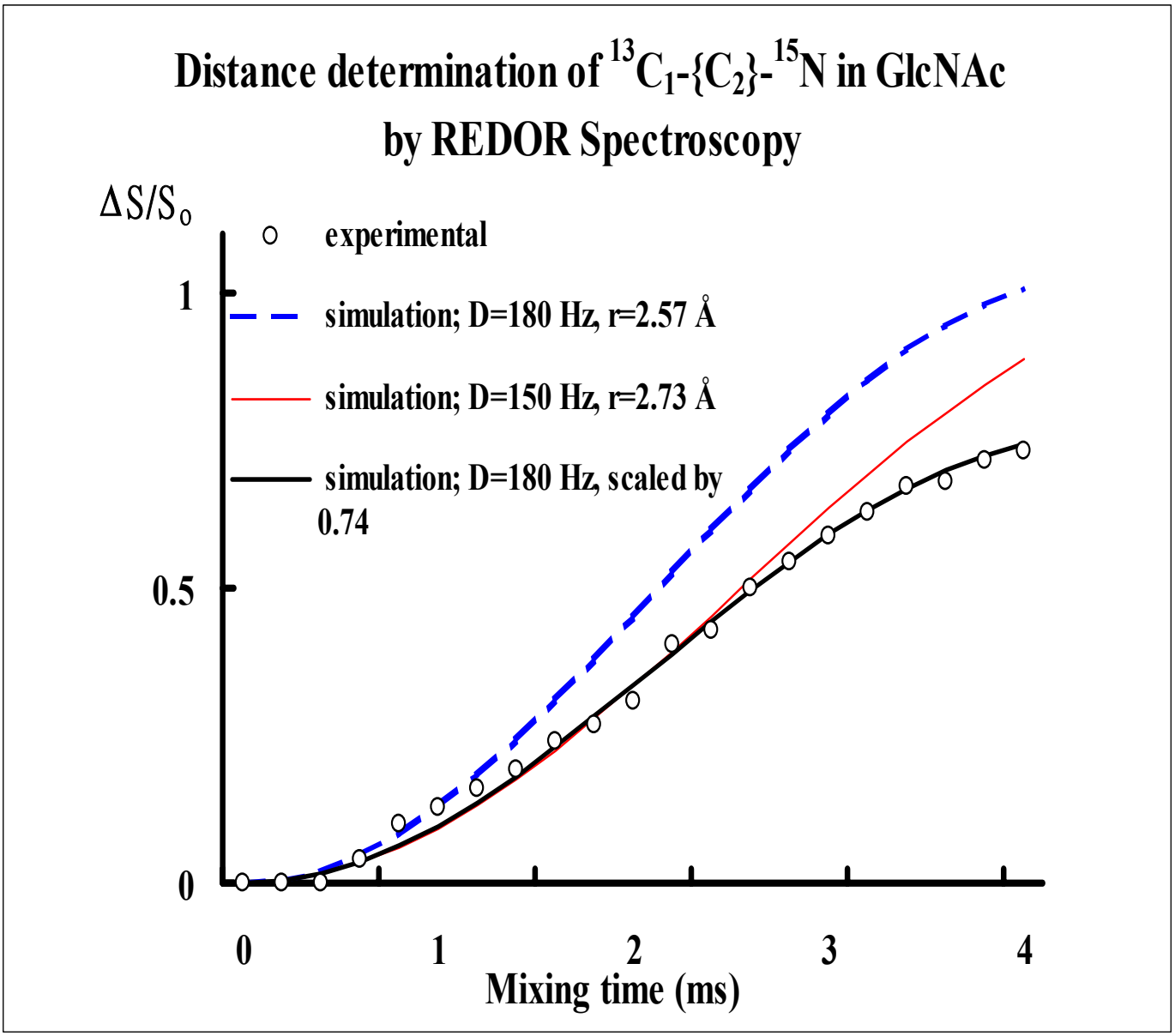
Distance determination of $^{13}C_1$-{C_2}-^{15}N in GlcNAc by REDOR Spectroscopy
ΔS/S0
experimental
simulation; D=180 Hz, r=2.57 Å
simulation; D=150 Hz, r=2.73 Å
simulation; D=180 Hz, scaled by 0.74
1
0.5
0
0
1
2
3
4
Mixing time (ms)

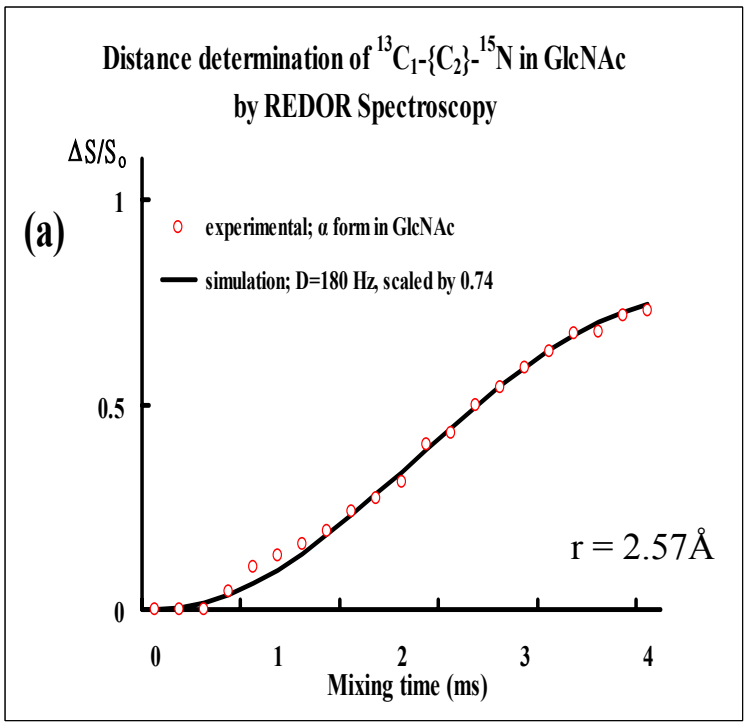
Distance determination of $^{13}C_1$-{C_2}-^{15}N in GlcNAc
by REDOR Spectroscopy
(a)
ΔS/S0
1
0.5
0
experimental; α form in GlcNAc
simulation; D=180 Hz, scaled by 0.74
r = 2.57Å
0
1
2
3
4
Mixing time (ms)

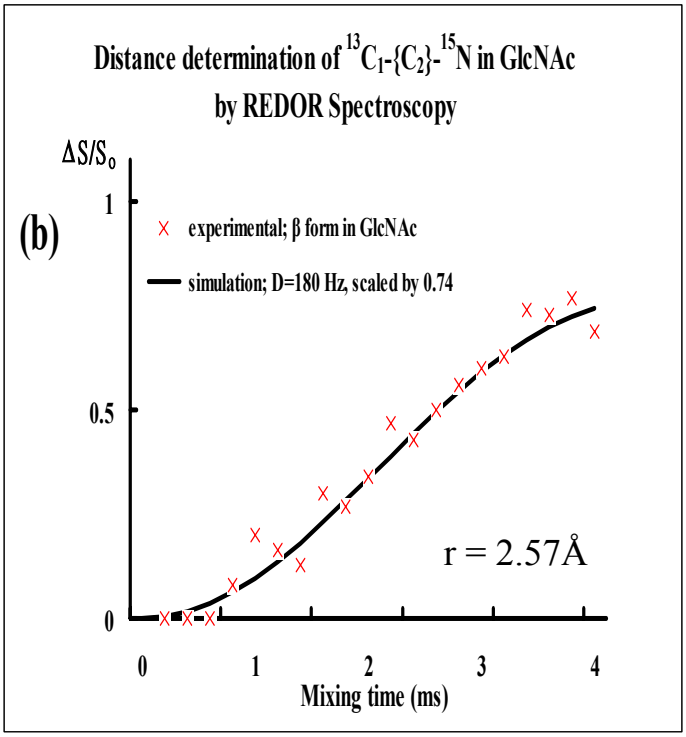
Distance determination of $^{13}C_1$-{C_2}-^{15}N in GlcNAc
by REDOR Spectroscopy
(b)
ΔS/S0
1
0.5
0
experimental; β form in GlcNAc
simulation; D=180 Hz, scaled by 0.74
r = 2.57Å
0
1
2
3
4
Mixing time (ms)

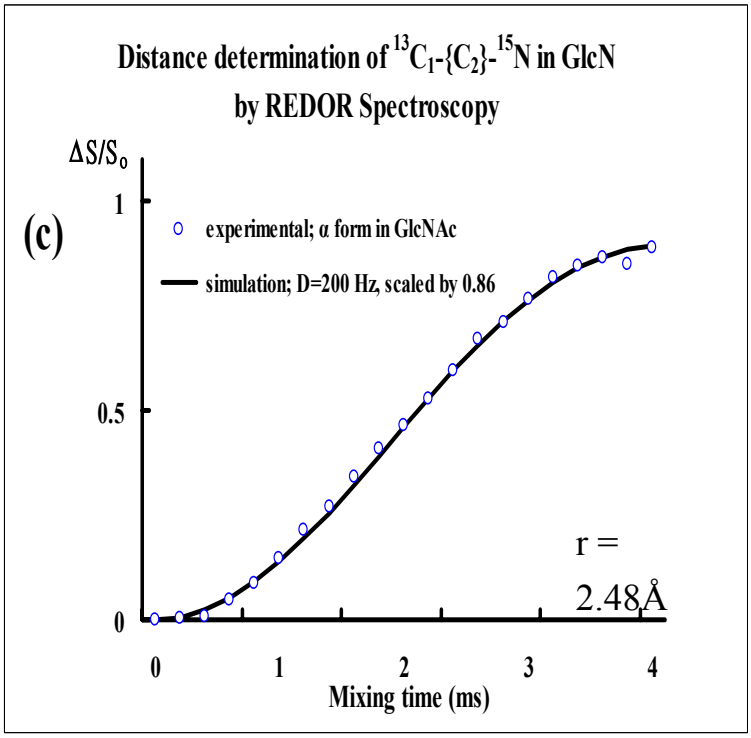
Distance determination of $^{13}C_1$-{C_2}-^{15}N in GlcN
by REDOR Spectroscopy
(c)
ΔS/S0
1
0.5
0
experimental; α form in GlcNAc
simulation; D=200 Hz, scaled by 0.86
r =
2.48Å
0
1
2
3
4
Mixing time (ms)

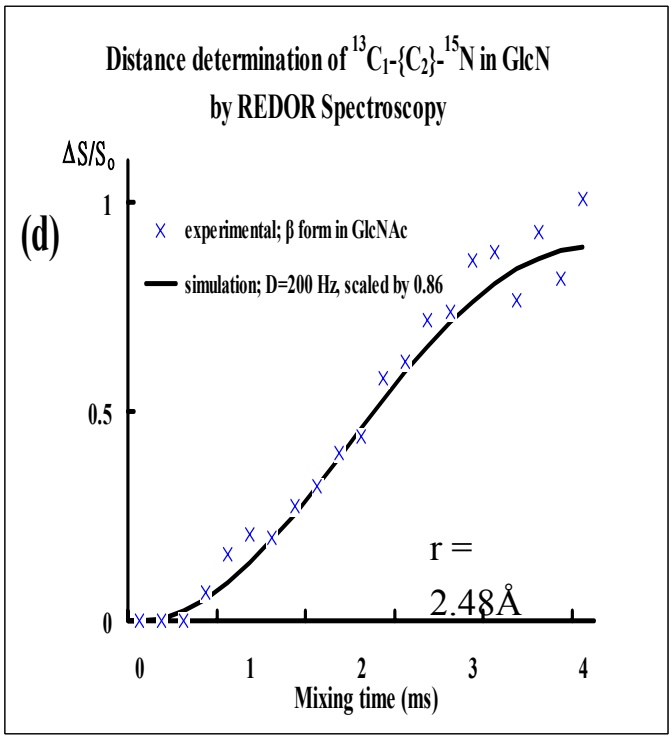
Distance determination of $^{13}C_1$-{C_2}-^{15}N in GlcN
by REDOR Spectroscopy
(d)
ΔS/S0
1
0.5
0
experimental; β form in GlcNAc
simulation; D=200 Hz, scaled by 0.86
r =
2.48Å
0
1
2
3
4
Mixing time (ms)

Table 2. $^{13}C_1$-^{15}N Distance Determination by Solid-state NMR REDOR Spectroscopy for the α and β anomers in GlcN and GlcNAc‡

	GlcN		GlcNAc	
	α	β	α	β
r† (Å)	2.48	2.48	2.57	2.57
D† (Hz)	200	200	180	180

‡Samples were specifically double-labeled with ^{13}C at the C_1 residue and with ^{15}N at the amide group attached to the C_2 residue. †Dipolar strength D is inversely proportional to the internuclear distance r to the third power, $D = \hbar \gamma_C \gamma_N / r^3$.

2D PISEMA (Polarization Inversion Spin Exchange at the Magic Angle experiment)

C. H. Wu, A. Ramamoorthy and S. J. Opella, J. Magn. Reson., A109, 270 (1994). Z.Gan, J. Magn. Reson., 143, 136 (2000).

Focus on the effect of neighboring protons on the spin exchange of a strongly coupled spin pair. By The dipolar couplings from the neighboring protons of a stongly coupled spin pair perturb the spin exchange only in the second order, therefore it has little contribution to the linewidth of PISEMA spectra in comparison to the separated-local-field spectra.

Dipolar splitting and Chemical shifts

$$\begin{aligned}\mathbf{F}(\rho, \tau) &= (\text{chemical shift}(\rho, \tau), \text{dipolar splitting}(\rho, \tau)) \\ &= (\sigma_{11}(-0.828 \cos\rho \sin\tau + 0.558 \sin\rho \sin\tau \\ &\quad - 0.047 \cos\tau)^2 + \sigma_{22}(0.554 \cos\rho \sin\tau \\ &\quad + 0.803 \sin\rho \sin\tau - 0.220 \cos\tau)^2 \\ &\quad + \sigma_{33}(-0.088 \cos\rho \sin\tau - 0.206 \sin\rho \sin\tau \\ &\quad - 0.975 \cos\tau)^2, \frac{\nu_{\|}}{2}(3(-0.326 \cos\rho \sin\tau \\ &\quad - 0.034 \sin\rho \sin\tau - 0.946 \cos\tau)^2 - 1))\end{aligned} \quad [1]$$

For a tilted helix, the plot of the PISA wheels is generated by graphing the set

$$S(\tau) = \{\mathbf{F}(\rho, \tau): \rho \in [0, 2\pi)\}. \quad [2]$$

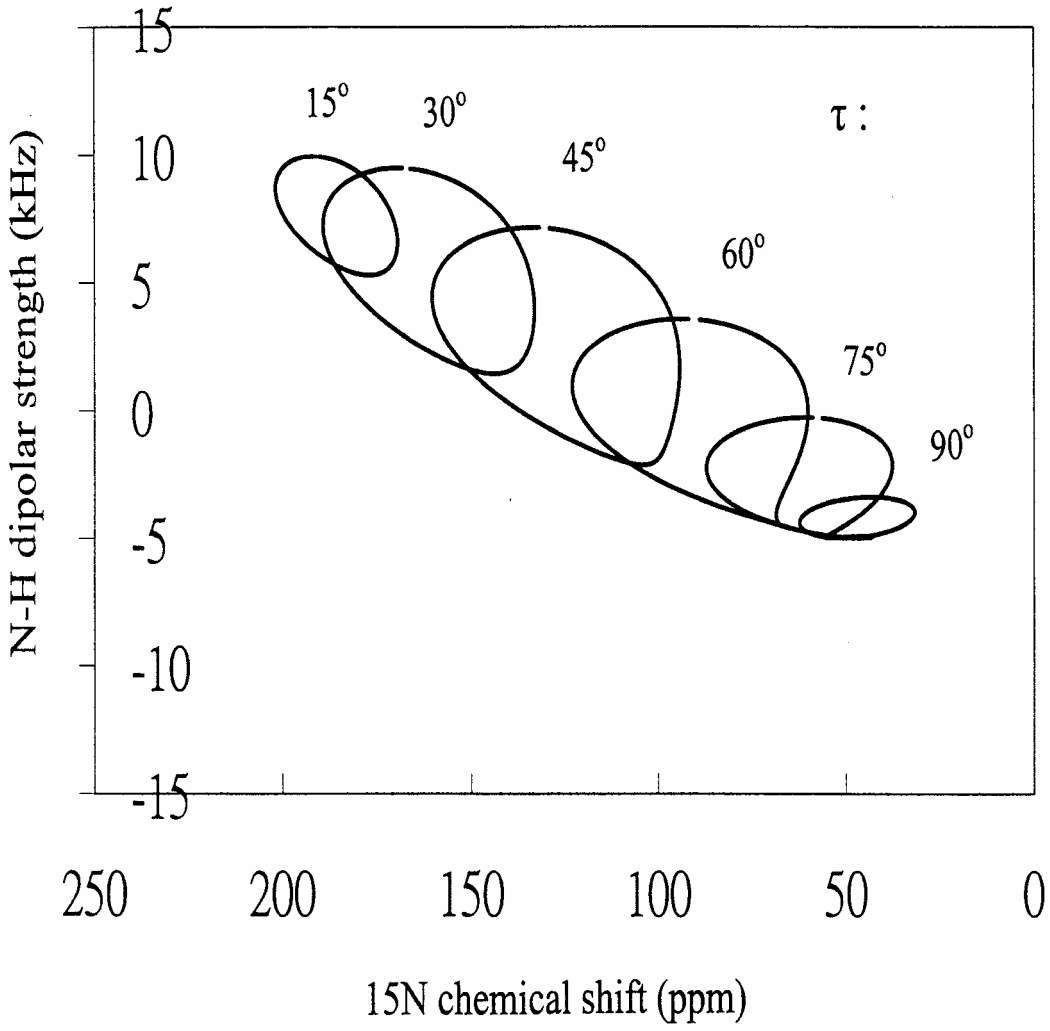

Fig. 4. "Circles" represents the wheel pattern corresponding to each tilted helix structure, where the slant angle was specific in figure. Average tensor elements (σ_{11}=31.3, σ_{22}=55.2, σ_{33}=201.8) in ppm, dipolar strength of 25 kHz and the relative orientation of the dipolar and chemical shift tensor of 17° were used in simulation.

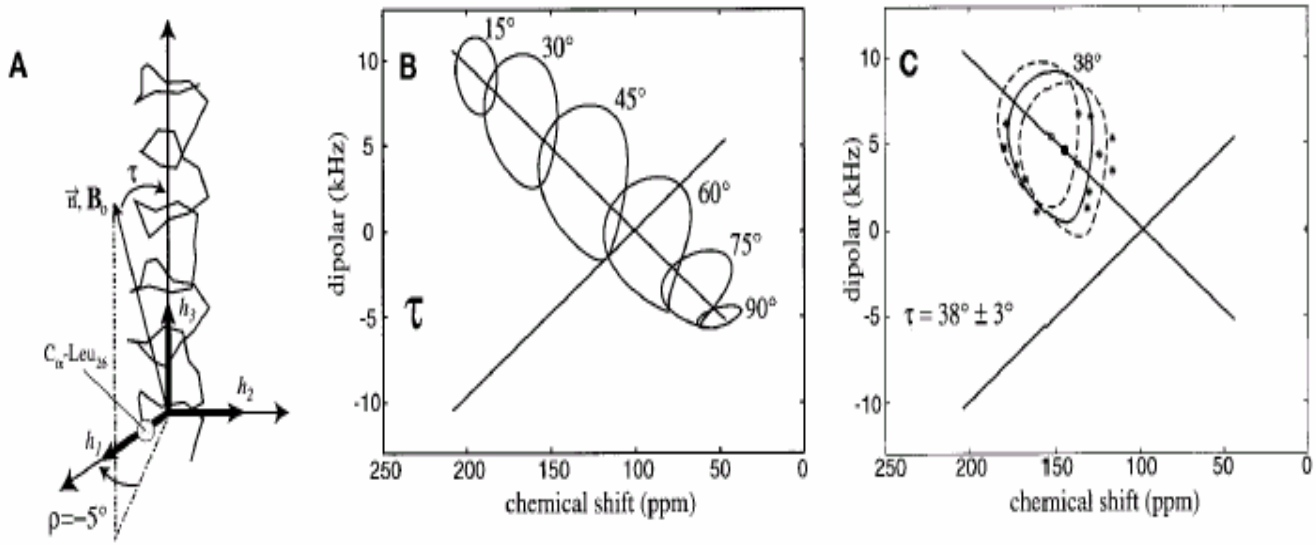

FIG. 2. The origins of the "PISA wheels." For the analysis in this manuscript, n, the bilayer normal, is always aligned parallel to B_0. (A) Definitions of τ and ρ for an α-helix. $\tau = 0°$ occurs when the helix axis, h_3, is parallel to B_0. $\rho = 0°$ occurs when the projection of B_0 onto a plane perpendicular to h_3 makes an angle of 0° with h_1, the radial axis of the helix that passes through the C_α carbon of Leu_{26}. (B) "Circles" drawn for one of the dipolar transitions using average values of tensor elements ($\tau_{11} = 31.3$, $\tau_{22} = 55.2$, $\sigma_{33} = 201.8$ ppm) and the relative orientations of the dipolar and chemical shift tensor, given by $\theta = 17°$, the angle in the peptide plane between σ_{33} and $\nu_{\parallel}$ (parallel to the N–H bond). The circles for the other dipolar transitions are the mirror image about 0 kHz. (C) Characterization of the M2-TMP helix tilt from a more complete set of PISEMA data than that presented in Fig. 1. The data are consistent with a helix tilt of 38 ± 3°. Note that the center of the PISA wheels falls on a line that passes through the isotropic chemical shift (96 ppm) at 0 kHz on the dipolar scale.

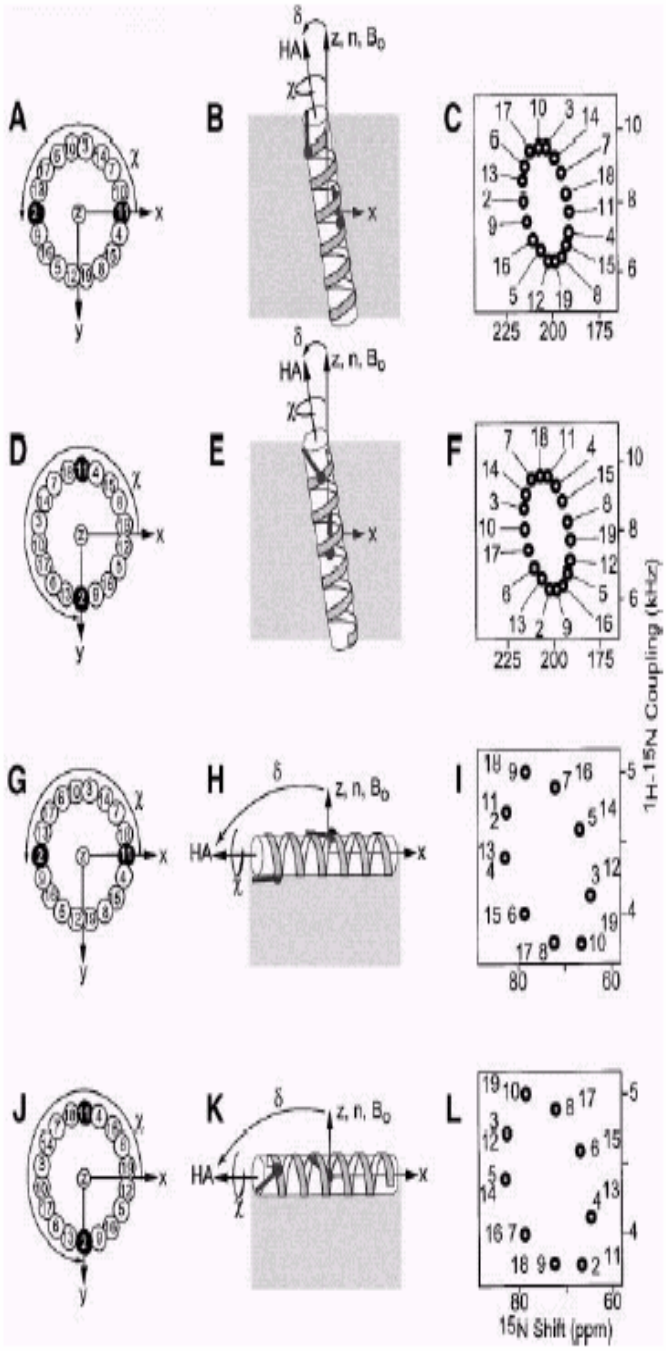

FIG. 3. Correspondence between membrane protein helix tilt and polarity, and the resulting PISEMA spectra for uniformly ^{15}N-labeled protein in oriented bilayers. A, D, G, and J. Helical wheels rotated by various values of the polar angle χ. B, E, H, and K. Helices rotated through various values of χ about their long axes (HA) and tilted by $\delta = 12°$ (B, E) and $\delta = 90°$ (H, K) away from the membrane normal (n). The *y* axis of the laboratory frame points out of the page. C, F, I, and L. Calculated PISEMA spectra for the various helix rotations and tilts. The NH bond vectors of the polar opposite residues 2 and 11 in the helical wheels are highlighted. The light gray areas in B, E, H, and K represent the lipid bilayer.

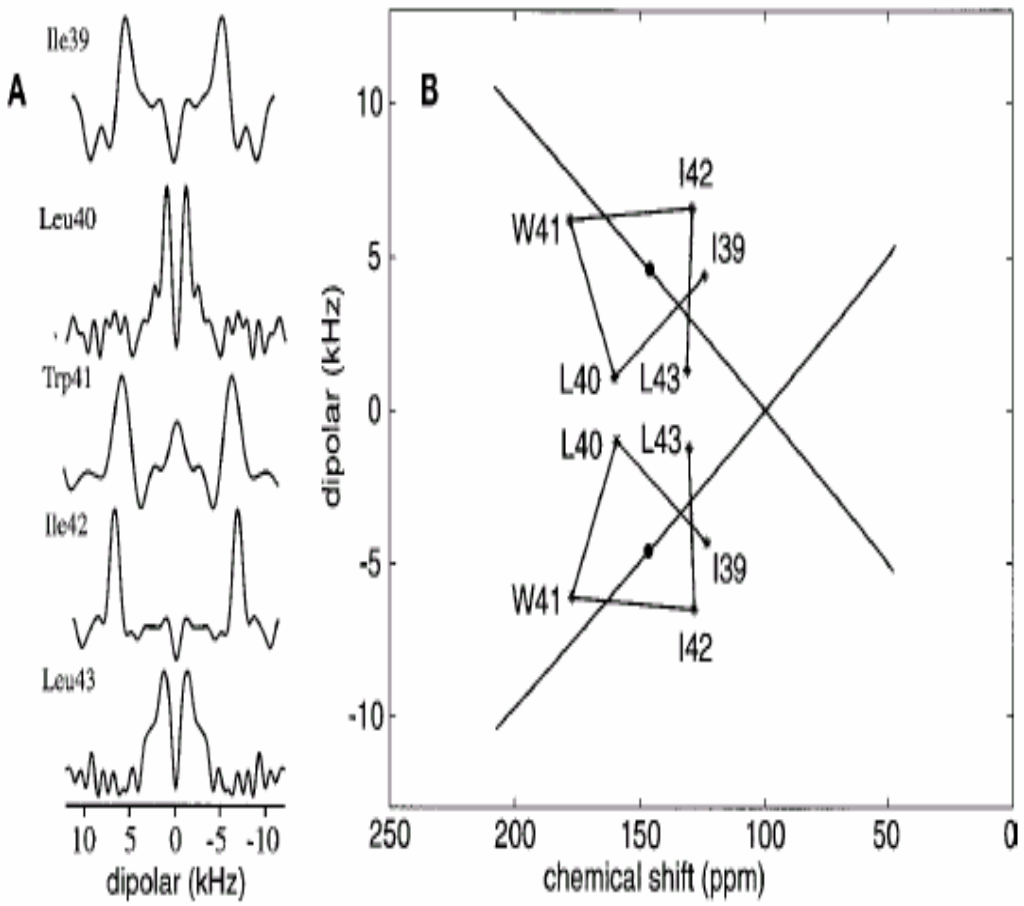

FIG. 1. (A) Dipolar splittings observed from PISEMA spectra of multiple and single site labeled preparations of M2-TMP in hydrated lipid bilayers aligned with the bilayer normal parallel to the magnetic field direction. The spectra were obtained (Song *et al.*, unpublished results) with a 400-MHz spectrometer using a Chemagnetics data acquisition system and a 9.4-T wide-bore Oxford Instruments magnet. An RF field strength of 38.5 kHz was used for the Lee–Goldburg (LG) condition corresponding to a LG time increment of 26 μs. A delay of 1 μs was given at the onset of each $\pm$LG cycle to compensate for the frequency synthesizer (PTS) switch time. The t_1 duration was incremented from 0 to 24 LG cycles and the refocused ^{15}N signal was typically acquired with 2000 transients for each t_1 increment. Spectral symmetry in the dipolar dimension was achieved by setting the imaginary part of the data to zero before the Fourier transform against t_1. The experimental error in the chemical shift dimension is $\pm$5 ppm and in the dipolar dimension it is $\pm$1 kHz. (B) Display of the dipolar splittings (*) at their observed chemical shift. The resonances are connected in helical wheel fashion. Since the two wheels are mirror images displaying identical information, only one will be used in the following figures.

Determination of rotational orientation of the helix, ρ

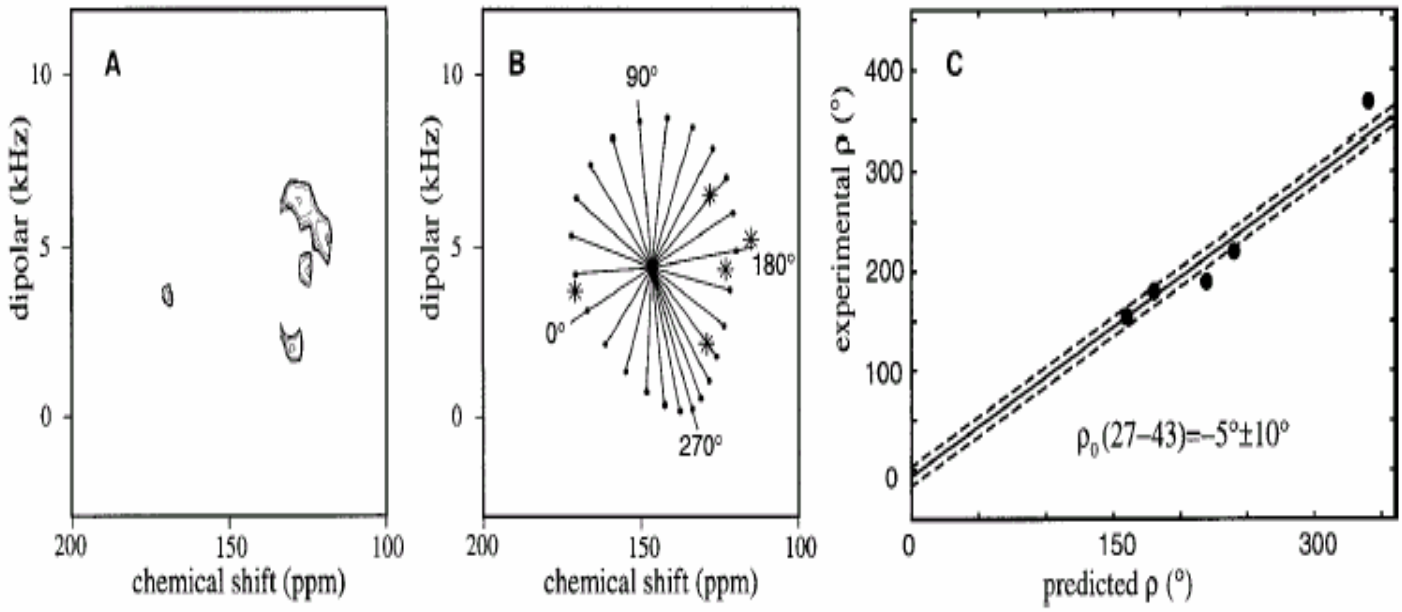

FIG. 3. (A) The ^{15}N Ile$_{32,33,35,39,42}$-labeled M2-TMP PISEMA spectrum obtained as in Fig. 1. Most of the resonances have been assigned based on single-site isotopic labels, but here the analysis has no dependence on such assignments. (B) Based on Eq. [1], the "PISA wheels" can be dissected into domains of ρ angles for cataloging an experimental value of ρ for each resonance. (C) The experimental ρ values are compared to predicted values based on residue number and 100°/residue for an ideal helix. Predicted and experimental values are paired by solving for a best fit. The result is an extrapolation and intersection with the experimental axis at $\rho_0 = -5 \pm 10°$.

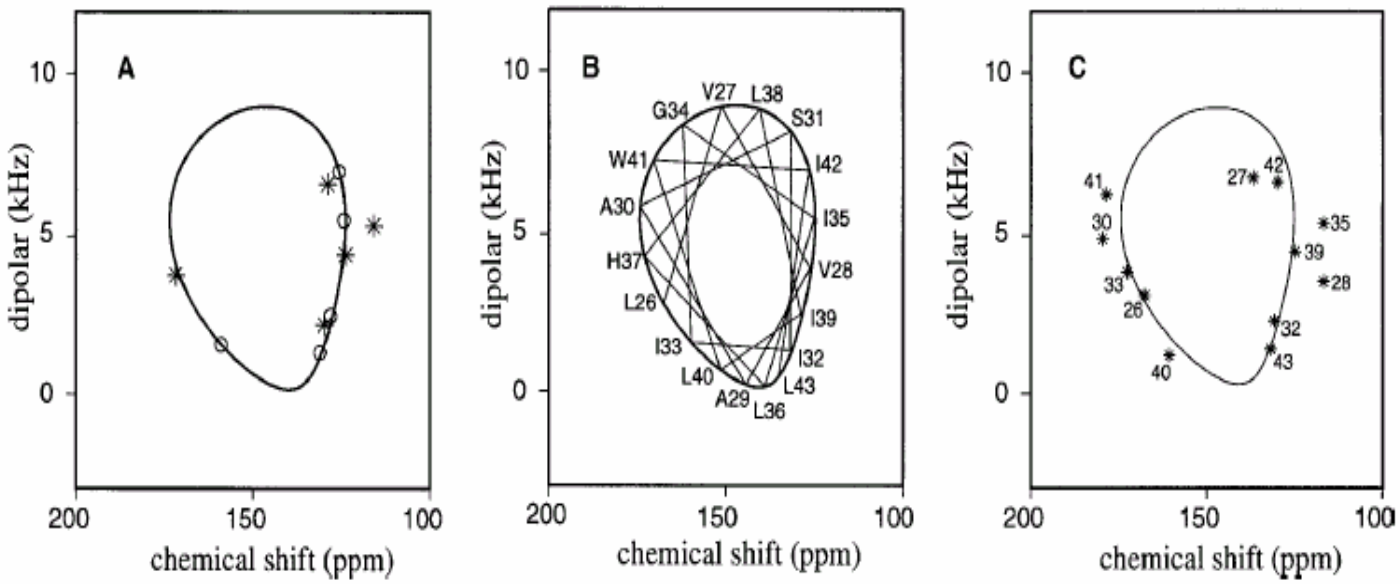

FIG. 4. (A) Best fit (○) to the 5-site Ile-labeled M2-TMP PISEMA resonances (*) based on the analysis in Fig. 3. (B) From this analysis and the resulting assignment of resonances, the helical wheel for this hydrophobic transmembrane peptide can be predicted. (C) The predicted resonance positions from the helical wheel are compared to the experimental data.

TABLE 1
Chemical Shift Tensor Element Magnitudes for the Observed Sites in M2-TMP[a]

Site	σ_{11}	σ_{22}	σ_{33}
Val27	33	55	198
Val28	29	53	202
Ile32	35	59	208
Ile33	31	54	202
Ile35	32	56	210
Ile39	30	54	195
Leu40	32	55	203
Trp41	32	56	205
Ile42	30	54	198
Leu43	29	56	200

[a] The chemical shift anisotropy has been determined from single site labeled samples of M2-TMP. Spectra were obtained of samples dried from trifluoroethanol where the peptide is observed to be α-helical; it is likely, therefore, that the peptides for this characterization are in the conformation of interest.

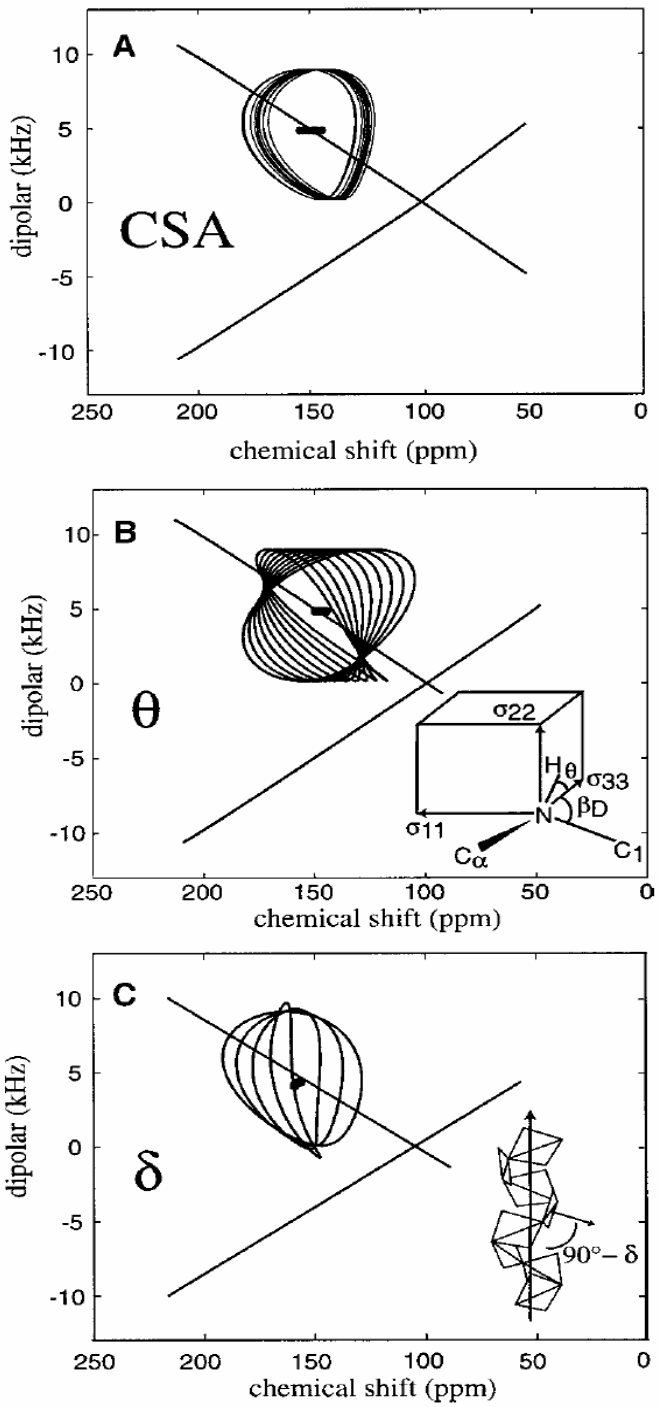

FIG. 5. The chemical shift anisotropy (CSA), relative orientation of chemical shift and dipolar tensors (θ), and local variation in helical structure through compensated peptide plane tilts (δ) are potential sources of distortion for the PISA wheel. (A) The chemical shift anisotropy has been determined from single site labeled samples of M2-TMP. The calculation of a "PISA wheel" using each of these CSA tensors (Table 1) is displayed showing significant variation in both the pattern and the calculation of its center. (B) The influence of θ on the PISA wheel is dramatic, but shows little effect on the pattern's center. The range of θ values displayed is 5 to 23° in 2° increments, where $\theta + \beta_D = 122°$, the HNC_1 bond angle. The value $\theta = 17°$ corresponding to $\beta_D = 105°$ has been used in all other figures. (C) The influence of peptide plane tilt on the shape of the PISA wheel is also dramatic, but there is little effect on the center of the pattern. The δ values displayed are 0, 5, 8.7, and 12°. The ideal helix has peptide plane tilts of $\delta = 8.7°$, the value used in all other figures.

(c) Quadrupolar Interaction

Quadrupolar Frequency

The quadrupolar frequency υ

$$\upsilon = \upsilon_0 \pm \frac{3}{8} C_Q \frac{1}{I(2I+1)} (\pm 2m_I + 1)[(3\cos^2\vartheta - 1) + \eta \sin^2\vartheta \cos 2\varphi]$$

where,

$C_Q = \frac{e^2 qQ}{h}$, describes quadrupolar constant

$$\eta = \frac{V_{11} - V_{22}}{V_{33}}$$

ϑ, φ : are the polar and azimuthal angles between the magnetic field direction and the quadrupolar vector.

$$\nu_{m,m-1} = \nu_o(1+\delta) - (2m-1)A + 1/\nu_o\{B[2I(I+1) - 3(2m^2-2m+1)] - C[4I(I+1) - 24m^2 + 24m - 9]\},$$

$$A = \nu_Q/2\,[(3/2 - 1/2\,\eta\cos2\phi)\cos^2\theta - 1/2\,(1 - \eta\cos2\phi)],$$

$$B = \nu^2_Q/288\,[(3 - \eta\cos2\phi)^2\cos^4\theta + (-18 + 4\eta^2 - 2\eta^2\cos^2 2\phi)\cos^2\theta + (3+\eta\cos2\phi)^2],$$

$$C = \nu^2_Q/72\,[-\cos^4\theta\,(3-\eta\cos2\phi)^2 + \cos^2\theta\,(9 - \eta^2 - 6\eta\cos2\phi + 2\eta^2\cos^2 2\phi) + \eta^2 - \eta^2\cos^2 2\phi],$$

where $\nu_o = \gamma_I Bo/2\pi$

$$\nu^2_Q = 3e^2qQ/\,h\,2I(2I-1)\text{ and}$$

$$\delta = \delta_{XX}\sin^2\theta\cos^2\phi + \delta_{YY}\sin^2\theta\sin^2\phi + \delta_{ZZ}\cos^2\theta - \delta_{XY}\sin^2\theta\sin2\phi - \delta_{XZ}\sin2\theta\cos\phi + \delta_{YZ}\sin2\theta\sin\phi$$

The angles θ, ϕ describe the orientation of the principal axes system of the quadrupolar tensor in the laboratory coordinate system. δ_{IJ} are the components of the chemical shift tensor in the quadrupolar tensor coordinate system.

For polycrystalline samples the line shape for each ($m \leftrightarrow m-1$) transition can be obtained by means of integration of the function $\nu_{m,m-1}\,P_m$ over ϕ from 0 to 2π with a coefficient $1/2\pi$ and over θ with a coefficient $\sin\theta/2$.

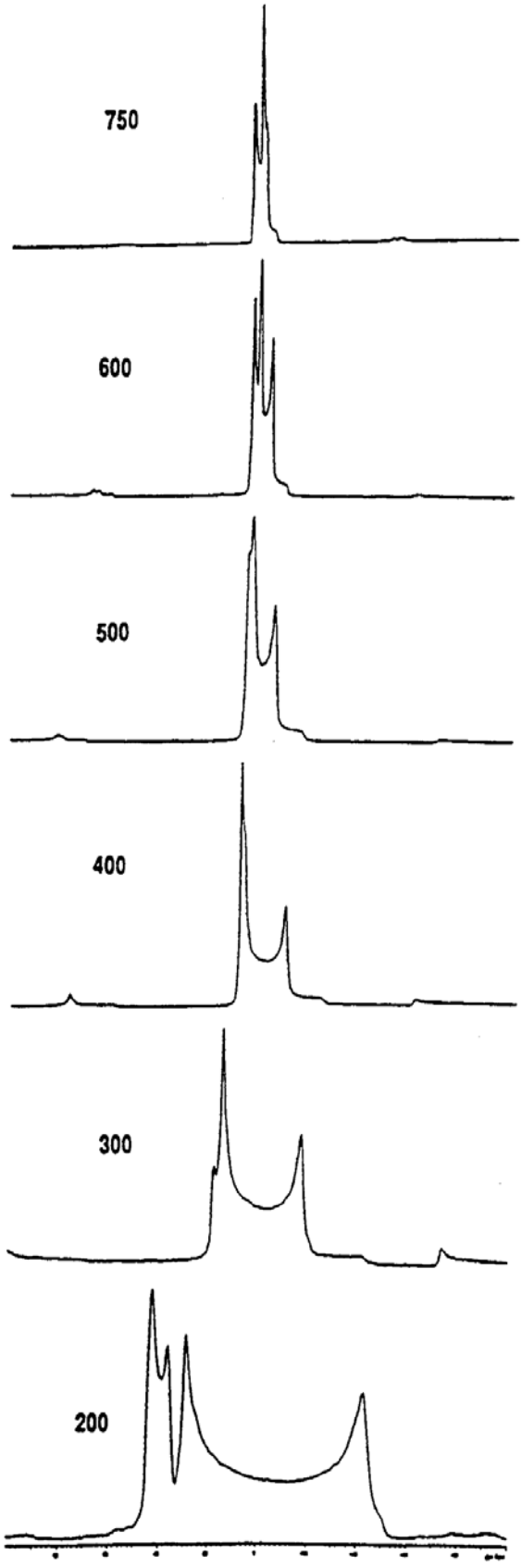

^{23}Na MAS spectra of Na_2MoO_4 at field strengths from 4.7 T to 17.6 T (200 to 750 MHz)

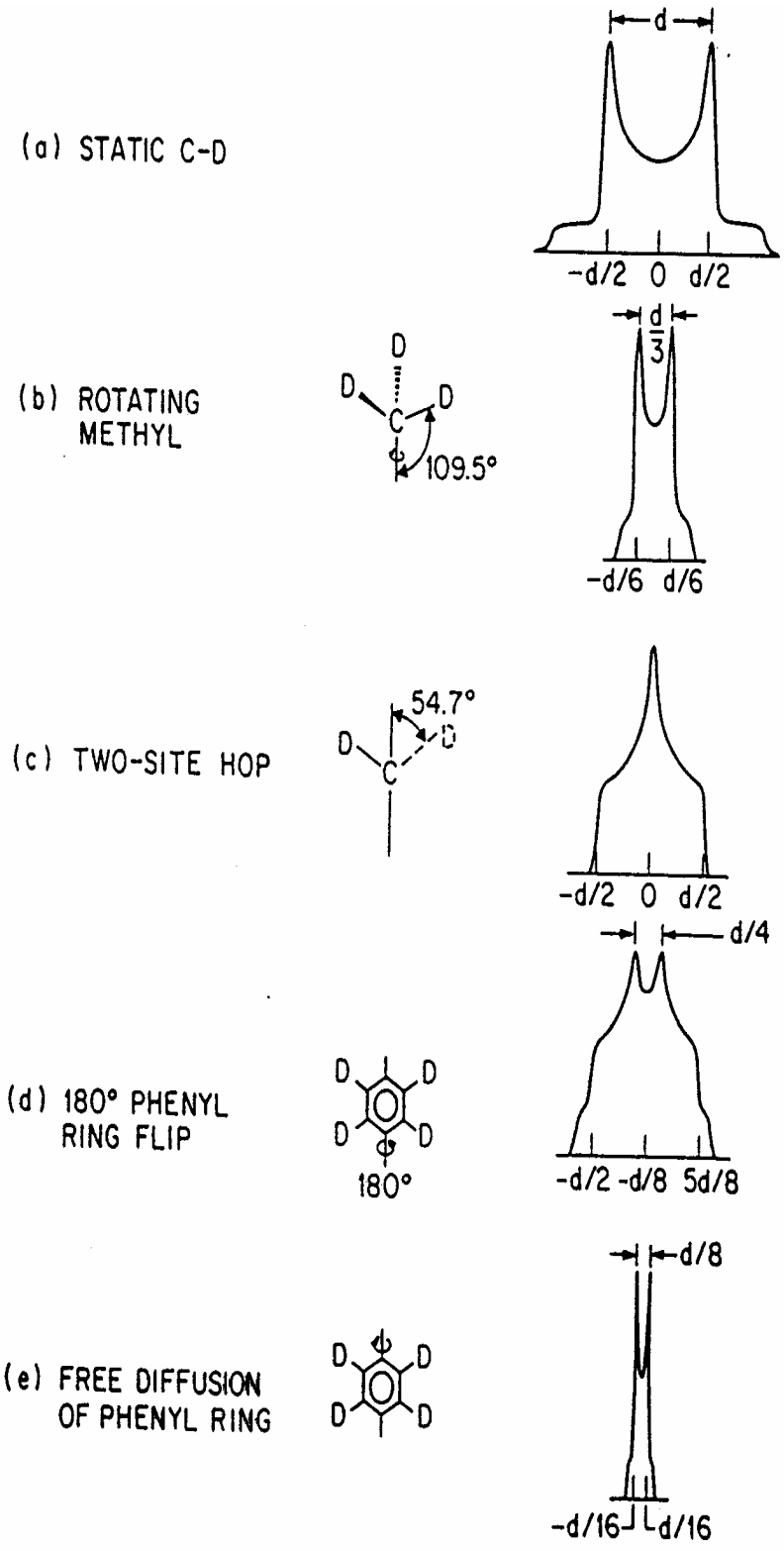

Figure 11.14 ■ Theoretical deuterium NMR lineshapes for various types of rapid ($\tau_c < 10^{-7}$ sec) anisotropic motions. [Reprinted with permission from Jelinski (1986).]

Multiple quantum solid-state NMR indicates a parallel, not antiparallel, organization of β-sheets in Alzheimer's β-amyloid fibrils

Oleg N. Antzutkin*†, John J. Balbach*, Richard D. Leapman‡, Nancy W. Rizzo‡, Jennifer Reed*, and Robert Tycko*§

*Laboratory of Chemical Physics, National Institute of Diabetes and Digestive and Kidney Diseases, National Institutes of Health, Bethesda, MD 20892-0520; †Division of Inorganic Chemistry, Luleå University of Technology, Luleå, Sweden S-971 87; and ‡Division of Bioengineering and Physical Science, Office of Research Services, National Institutes of Health, Bethesda, MD 20892

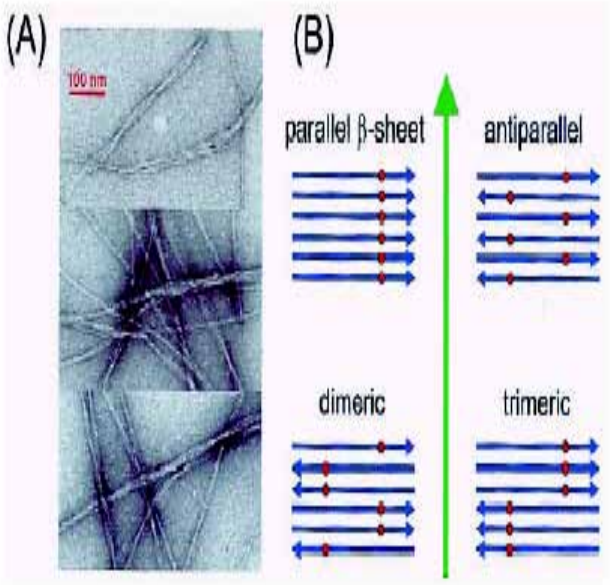

Fig. 1. (*A*) Electron micrographs of negative-stained $A\beta_{1-40}$ fibrils adsorbed to carbon films from an $A\beta_{1-40}$ solution after incubation at 24°C and pH 7.4 for 3 days. Typical amyloid fibrils are observed, appearing as single filaments or bundles of filaments with overall diameters ranging from 8 to 20 nm and with twist periodicities between 40 and 150 nm. The same solution, in which the $A\beta_{1-40}$ peptides were labeled with ^{13}C at the methyl carbon of Ala-21, subsequently was lyophilized for MQNMR measurements shown in Fig. 2. (*B*) $A\beta_{1-40}$ fibrils are believed to have a predominantly β-sheet structure with peptide chains (blue arrows) approximately perpendicular to and hydrogen bonds approximately parallel to the long axis of the fibril (green arrow). Four candidates for the supramolecular organization of the fibrils are shown. These can be distinguished experimentally by incorporating ^{13}C labels (red dots) at a single site in the peptide and measuring ^{13}C multiple quantum NMR spectra, because observation of an *n*-quantum signal requires that at least *n* ^{13}C nuclei be close enough in space to have significant magnetic dipole-dipole couplings.

Materials and Methods

Sample Preparation. Peptides with the human $A\beta_{1-40}$ sequence DAEFRHDSGYEVHHQKLVFFAEDVGSNKGAIIGLM-VGGVV were synthesized, purified, and fibrillized from 0.25- to 1.0-mM solutions at pH 7.4 as described (11, 12). Fibrillized solutions were lyophilized for solid state NMR measurements. Typical solid state NMR samples were 10 mg. For EM, fibrillized solutions were diluted by a factor of 10–20 and negatively stained with uranyl acetate as described (11, 13).

The following samples were synthesized with uniform ^{15}N and ^{13}C labeling of the specified residues: SU7 (F19, V24, G25, A30, I31, L34, M35), SU6 (A2, D7, G9, Y10, V12, M35), SU5 (D23, K28, G29, I32, V36), and CU6 (K16, L17, V18, F19, F20, A21). The following samples were synthesized with ^{13}C labels at the specified pairs of backbone carbonyl sites: DL1 (D23, V24), DL2 (V24, G25), DL3 (G25, S26), DL4 (K28, G29), and DL5 (G29, A30). The notations SUn, CUn, and DLn indicate "scattered uniform" labeling of *n* residues, "consecutive uniform" labeling of *n* residues, and the *n*th "double labeled" sample, respectively.

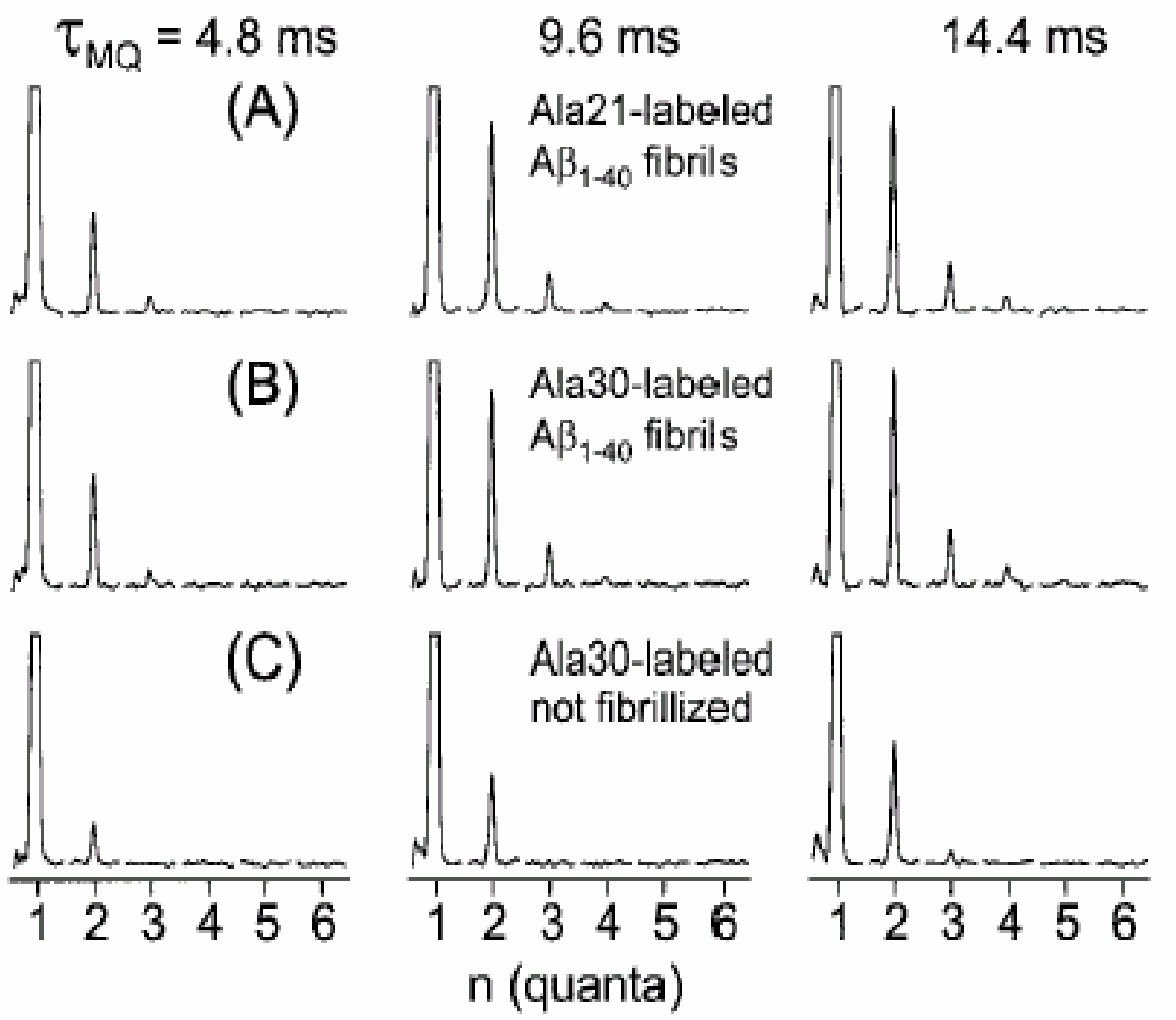

Fig. 2. ^{13}C MQNMR spectra of fibrillized and unfibrillized $A\beta_{1-40}$ samples, shown in order of increasing MQ excitation time τ_{MQ}. Each MQ spectrum is displayed as a series of subspectra for MQ orders from 1 to 6, with a spectral window from −15 kHz to + 15 kHz in each subspectrum. Vertical scales are adjusted so that one-quantum peaks are clipped at 25% of their maximum values. In the fibrillized samples (*A* and *B*), the amplitudes of two-, three-, and four-quantum signals increase with increasing τ_{MQ}. Spectra of samples with ^{13}C labels at methyl carbons of Ala-21 and Ala-30 are nearly identical. In unfibrillized samples (*C*), the three-quantum amplitude is small and no four-quantum signal is observed.

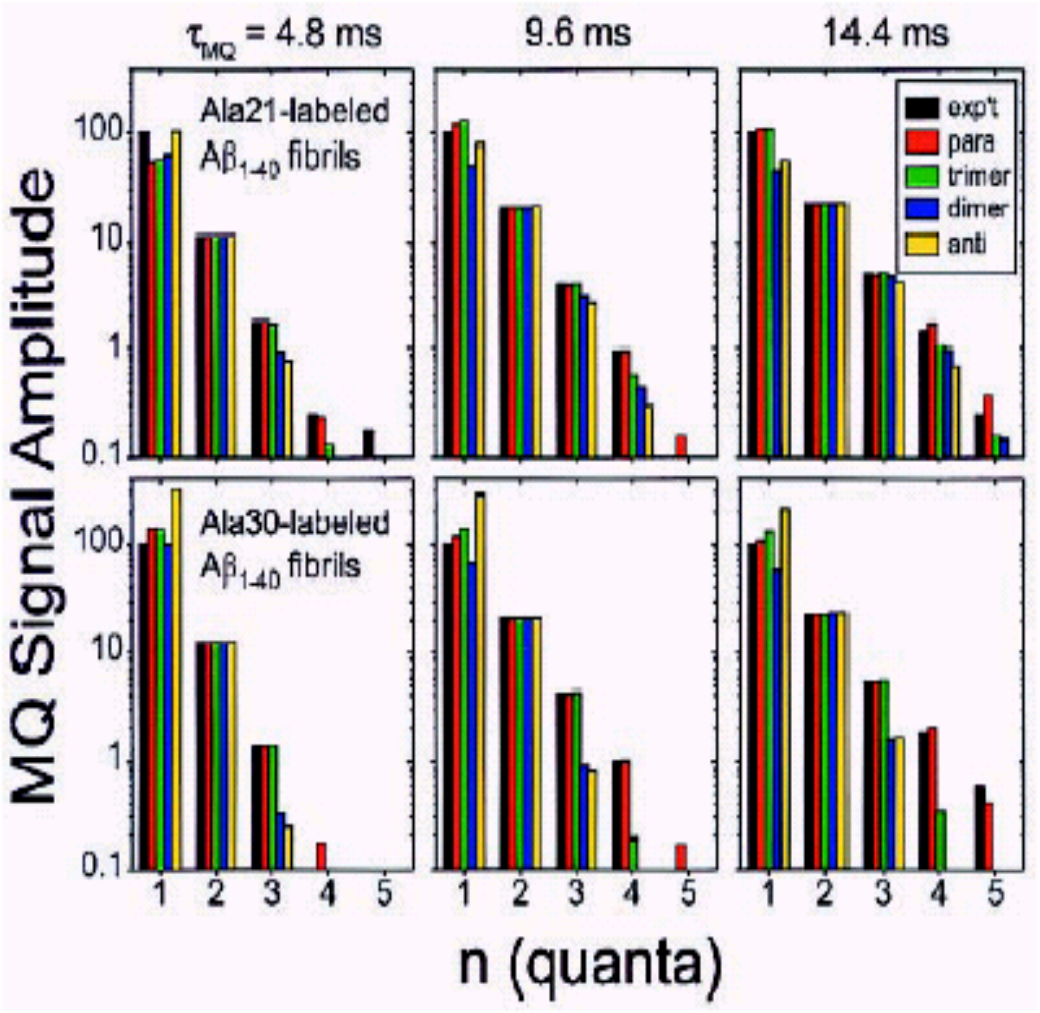

Fig. 3. Comparison of experimental MQNMR amplitudes (black) with simulations for parallel (red), trimeric (green), dimeric (blue), and antiparallel organizations of β-sheets in $A\beta_{1-40}$ fibrils, for samples labeled with ^{13}C at methyl carbons of Ala-21 and Ala-30. Experimental MQNMR amplitudes are normalized to a one-quantum amplitude of 100. A logarithmic vertical scale is required because the amplitudes vary over 2 orders of magnitude. The parallel β-sheet model fits all of the experimental data most closely. Experimental amplitudes were determined from MQNMR spectra in Fig. 2 by integrating each subspectrum over the interval from −2 kHz to +3 kHz. Uncertainties in the experimental amplitudes, evaluated as the rms noise integrated over a 5-kHz-wide interval, are ±0.11, ±0.14, and ±0.14 for the Ala-21-labeled $A\beta_{1-40}$ fibril data, and ±0.15, ±0.17, and ±0.24 for the Ala-30-labeled $A\beta_{1-40}$ fibril data, for τ_{MQ} = 4.8 ms, 9.6 ms, and 14.4 ms, respectively.

A structural model for Alzheimer's β-amyloid fibrils based on experimental constraints from solid state NMR

Aneta T. Petkova*, Yoshitaka Ishii*†, John J. Balbach*, Oleg N. Antzutkin‡, Richard D. Leapman§, Frank Delaglio*, and Robert Tycko*¶

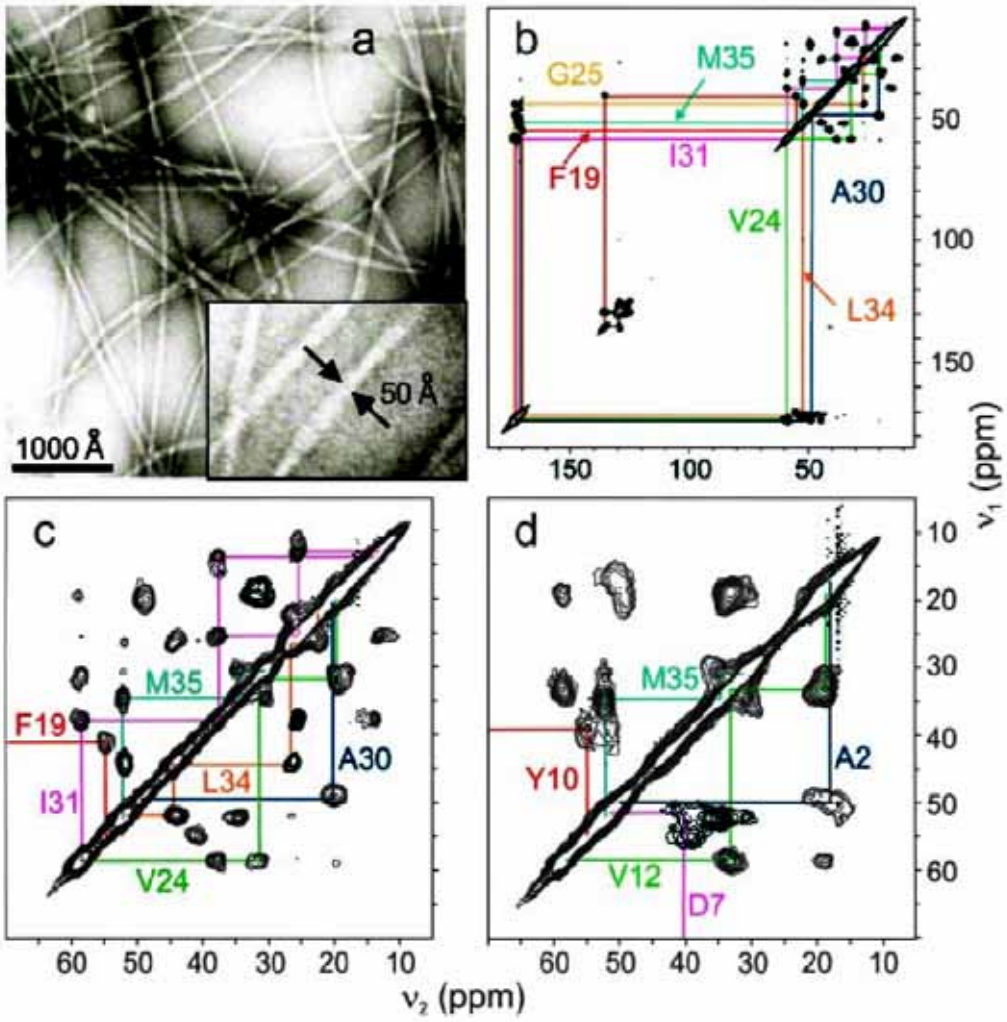

Fig. 1. (*a*) Transmission electron microscope images of negatively stained amyloid fibrils after 14-day incubation of a 0.5 mM $A\beta_{1-40}$ solution. A 3× expansion (*Inset*) shows fibrils with the smallest diameters observed. (*b*) 2D ^{13}C-^{13}C chemical shift correlation spectrum of $A\beta_{1-40}$ fibril sample SU7, showing resonance assignment paths for the seven uniformly ^{15}N- and ^{13}C-labeled residues in this sample. (*c*) Expansion of the aliphatic region of the 2D spectrum of SU7. (*d*) Aliphatic region of the 2D ^{13}C-^{13}C chemical shift correlation spectrum of $A\beta_{1-40}$ fibril sample SU6.

Table 1. ^{13}C and ^{15}N NMR chemical shift values (ppm) for ^{13}C- and ^{15}N-labeled sites in $A\beta_{1-40}$ fibrils, referenced to TMS (tetramethylsilane) or liquid NH_3

Residue	CO	C_α	C_β	C_γ	C_δ	C_κ	C_ζ, N_ζ	N	Sample
A2	173.7	49.9	18.2					ND	SU6
	(176.1)	(50.8)	(17.4)						
D7	~173.0	51.5	40.4	177.9				120.6	SU6
	(174.6)	(52.5)	(39.4)	(178.3)				(120.4)	
G9	169.3	42.9						107.2	SU6
	(173.2)	(43.4)						(108.8)	
Y10	172.0	55.0	39.5	126.5	130.7	116.5	156.2	122.4	SU6
	(174.2)	(56.2)	(37.1)	(128.9)	(131.6)	(116.5)	(155.6)	(120.3)	
V12	173.0	58.7	33.2	18.8, 18.8				127.0	SU6
	(174.6)	(60.5)	(31.2)	(19.4, 18.6)				(119.2)	
K16	171.5	52.7	34.1	24.0	28.6	39.8	33.7	ND	CU6
			36.9	24.8					
	(174.9)	(54.5)	(31.4)	(23.0)	(27.3)	(40.2)	(32.7)		
L17	172.8	52.3	~44.5	26.0	~24.4, ~23.3			ND	CU6
	173.0	51.6	~40.8	~27.0	~24.8, ~23.1				
	(175.9)	(53.4)	(40.7)	(25.2)	(23.2, 21.6)				
V18	170.3	58.9	33.6	19.2				121.7	CU6
	(174.6)	(60.5)	(31.2)	(19.4, 18.6)				(119.2)	
F19	170.2	55.3	41.0	135.7	129.6	129.6	125.8	130.5	CU6, SU7
	(174.1)	(56.0)	(37.9)	(137.2)	(130.2)	(129.8)	(128.2)	(120.3)	
F20	170.2	54.6	41.0	135.7	129.2	129.2	125.8	ND	CU6
	(174.1)	(56.0)	(37.9)	(137.2)	(130.2)	(129.8)	(128.2)		
A21	172.7	48.2	21.0					130.9	CU6
	174.0	48.0	18.9					126.3	
	(176.1)	(50.8)	(17.4)					(123.8)	
D23	173.1	51.0	41.9	180.2				118.5	SU5
	174.1	52.4	39.4	178.0				123.3	
	(174.6)	(52.5)	(39.4)	(178.3)				(120.4)	
V24	173.8	58.6	31.3	19.9, 18.3				125.0	SU7
	173.6	59.0	32.8	19.9, 19.9				125.0	
	(174.6)	(60.5)	(31.2)	(19.4, 18.6)				(119.2)	
G25	174.2	44.4						113.9	SU7
	171.1	46.9						117.8	
	171.1	~44.2						113.9	
	(173.2)	(43.4)						(108.8)	
K28	174.3	52.8	35.6	24.7	27.8	42.0	33.0	119.5	SU5
	172.4	53.5	33.4	22.3	28.5	39.1	32.9	112.7	
	(174.9)	(54.5)	(31.4)	(23.0)	(27.3)	(40.2)	(32.7)	(120.4)	
G29	172.4	47.2						117.0	SU5
	168.6	42.4						104.1	
	(173.2)	(43.4)						(108.8)	
A30	173.2	48.4	20.5					122.1	SU7
								127.4	
	171.3	49.5	20.5					119.2	
	(176.1)	(50.8)	(17.4)					(123.8)	
I31	172.5	58.4	38.0	25.7, 13.8	13.3			120.6	SU7
	(174.7)	(59.4)	(37.1)	(25.5, 15.7)	(11.2)			(119.9)	
I32	173.8	56.7	40.2	25.2, 15.9	12.4			125.0	SU5
	172.2	57.0	38.7	24.6, 15.3	12.1			125.0	
	(174.7)	(59.4)	(37.1)	(25.5, 15.7)	(11.2)			(119.9)	
L34	171.0	52.1	44.8	27.0	~24.0, 22.5			~128.0	SU7
			44.1	26.3	24.0, 22.9			~128.0	
	(175.9)	(53.4)	(40.7)	(25.2)	(23.2, 21.6)			(121.8)	
M35	171.2	52.1	34.6	30.8		16.7		125.4	SU7, SU6
	(174.6)	(53.7)	(31.2)	(30.3)		(15.2)		(119.6)	
V36	171.8	58.8	31.9	18.9				126.6	SU5
	(174.6)	(60.5)	(31.2)	(19.4, 18.6)				(119.2)	

Values preceded by ~ have an uncertainty of 0.6 ppm. Otherwise, the uncertainty is 0.3 ppm. Values that could not be determined are indicated by ND. Values in parentheses are random-coil shifts, taken from Wishart *et al.* (51) and adjusted to the TMS reference.

TABLE IX

CHEMICAL SHIFT VALUES FOR BACKBONE ATOMS USED IN DETERMINATION OF SECONDARY STRUCTURE[a]

Residue	α-^{1}H range	2-^{13}C range	1-^{13}C range
Ala	4.35 ± 0.10	52.2 (+0.8, −0.5)	177.6 ± 0.5
Cys	4.65 ± 0.10	56.8 (+0.8, −0.5)	174.1 ± 0.5
Asp	4.76 ± 0.10	53.9 (+0.8, −0.5)	176.8 ± 0.5
Glu	4.29 ± 0.10	56.5 (+0.8, −0.5)	176.6 ± 0.5
Phe	4.66 ± 0.10	57.9 (+0.8, −0.5)	175.5 ± 0.5
Gly	3.97 ± 0.10	45.0 (+0.8, −0.5)	173.6 ± 0.5
His	4.63 ± 0.10	55.5 (+0.8, −0.5)	174.9 ± 0.5
Ile	3.95 ± 0.10	61.2 (+0.8, −0.5)	176.5 ± 0.5
Lys	4.36 ± 0.10	56.5 (+0.8, −0.5)	176.5 ± 0.5
Leu	4.17 ± 0.10	55.0 (+0.8, −0.5)	176.9 ± 0.5
Met	4.52 ± 0.10	55.2 (+0.8, −0.5)	177.0 ± 0.5
Asn	4.75 ± 0.10	52.7 (+0.8, −0.5)	175.6 ± 0.5
Pro	4.44 ± 0.10	63.0 (+0.8, −0.5)	176.0 ± 0.5
Gln	4.37 ± 0.10	56.0 (+0.8, −0.5)	175.6 ± 0.5
Arg	4.38 ± 0.10	56.0 (+0.8, −0.5)	176.6 ± 0.5
Ser	4.50 ± 0.10	58.1 (+0.8, −0.5)	174.7 ± 0.5
Thr	4.35 ± 0.10	62.0 (+0.8, −0.5)	175.5 ± 0.5
Val	3.95 ± 0.10	62.2 (+0.8, −0.5)	176.0 ± 0.5
Trp	4.70 ± 0.10	57.6 (+0.8, −0.5)	175.6 ± 0.5
Tyr	4.60 ± 0.10	58.0 (+0.8, −0.5)	175.9 ± 0.5

[a] Data are given in ppm, relative to DSS.

Structural information deduced from solid state NMR spectroscopy

- Secondary shifts are strongly correlated with peptide or protein backbone conformation. In particular, values for β-strand segments are characteristically negative for $^{13}C_{\alpha}$ and ^{13}CO sites and positive for $^{13}C_{\beta}$ sites.

- Multiplicity of chemical shifts was attributed to the differences in molecular structure associated with the differences in fibril morphology.

- ^{13}C chemical shifts for D23, V24, G25 and G29 are inconsistent with expectations for a β-strand. Thus, the chemical shift data qualitatively suggest a conformation for the structurally ordered part of $A_{\beta 1\text{-}40}$ consisting of two β-strands that are separated by a bend or loop contained within residues 23-29. The conformation in the bend segment may vary with fibril morphology and fibrillization conditions.

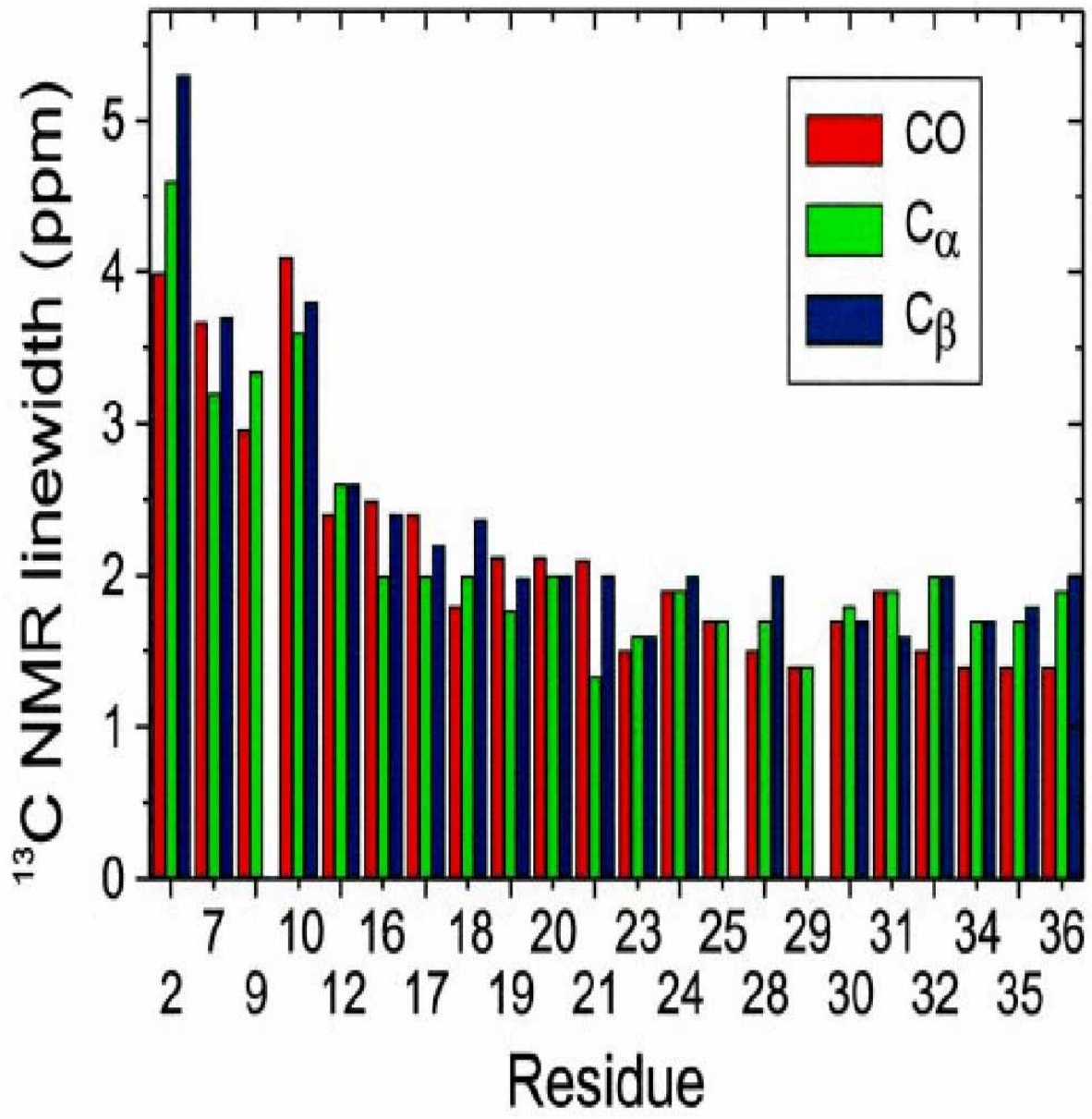

Fig. 2. ^{13}C NMR linewidths for CO, Cα, and Cβ sites in Aβ_{1-40} fibrils, determined from 2D solid state NMR spectra as in Fig. 1. Linewidths of 2.5 ppm or less indicate well-ordered conformations. Larger linewidths in the N-terminal segment indicate structural disorder.

Structural information deduced from solid state NMR spectroscopy

- Secondary shifts $\Delta\delta \equiv \delta_{fibril} - \delta_{coil}$ are strongly correlated with peptide or protein backbone conformation. In particular, values for β-strand segments are characteristically negative for $^{13}C_{\alpha}$ and ^{13}CO sites and positive for $^{13}C_{\beta}$ sites.

- Multiplicity of chemical shifts was attributed to the differences in molecular structure associated with the differences in fibril morphology.

- ^{13}C chemical shifts for D23, V24, G25 and G29 are inconsistent with expectations for a β-strand. Thus, the chemical shift data qualitatively suggest a conformation for the structurally ordered part of $A_{\beta 1\text{-}40}$ consisting of two β-strands that are separated by a bend or loop contained within residues 23-29. The conformation in the bend segment may vary with fibril morphology and fibrillization conditions.

- Linewidths in the 1.5-2.5 ppm range in solid state ^{13}C MAS NMR spectra are characteristic of well-structured peptide in rigid noncrystalline environments, whereas significantly larger linewidths are observed in disordered biopolymers shows that the N-terminal segment of $A_{\beta 1\text{-}40}$ is disordered in the fibrils.

Table 2. Residue-specific ϕ and ψ backbone torsion angles (degrees) for Aβ_{1-40} fibrils, predicted from ^{13}C and ^{15}N chemical shifts in Table 1 or determined from measurements on the doubly ^{13}C-labeled DLn samples

Residue	ϕ, ψ from chemical shift set 1*	ϕ, ψ from chemical shift set 2†	ϕ, ψ from DLn samples
G9	−148 ± 11, 151 ± 15	−148 ± 11, 151 ± 15	
Y10	−127 ± 9, 124 ± 9	−127 ± 9, 124 ± 9	
V12	−119 ± 8, 124 ± 10	−119 ± 8, 124 ± 10	
K16	−149 ± 12, 152 ± 8	−149 ± 12, 152 ± 8	
L17	−150 ± 12, 143 ± 9	−150 ± 12, 143 ± 9	
V18	−145 ± 9, 147 ± 11	−145 ± 8, 146 ± 12	
F19	−144 ± 10, 141 ± 12	−144 ± 10, 139 ± 15	
F20	−147 ± 9, 151 ± 11	−145 ± 11, 152 ± 13	
A21	−137 ± 12, 143 ± 16	−127 ± 11, 141 ± 19	
D23	−145 ± 16, 147 ± 16	−83 ± 13, 122 ± 22	
V24	−103 ± 10, 117 ± 11	−100 ± 12, 114 ± 22	−145, 115
G25	−88 ± 30, 124 ± 33	−58 ± 48, 11 ± 74	−70, −40
S26			68, −65
K28	−134 ± 12, 152 ± 14	−151 ± 14, 156 ± 13	
G29	−59 ± 50, 119 ± 58	−150 ± 18, 156 ± 14	−120, −125
A30	−138 ± 14, 157 ± 14	−144 ± 12, 145 ± 13	−165, 133
I31	−113 ± 16, 127 ± 12	−118 ± 15, 129 ± 11	
I32	−123 ± 10, 146 ± 14	−127 ± 9, 147 ± 12	
L34	−143 ± 9, 145 ± 17	−144 ± 8, 145 ± 16	
M35	−141 ± 9, 138 ± 11	−141 ± 9, 138 ± 11	
V36	−118 ± 8, 120 ± 11	−118 ± 8, 120 ± 11	

*First chemical shift value for each labeled site in Table 1.

†Second chemical shift value for each labeled site in Table 1, where more than one value is observed.

(c) Distance d_{NN} and torsion angles relationship – Ramachandran plot

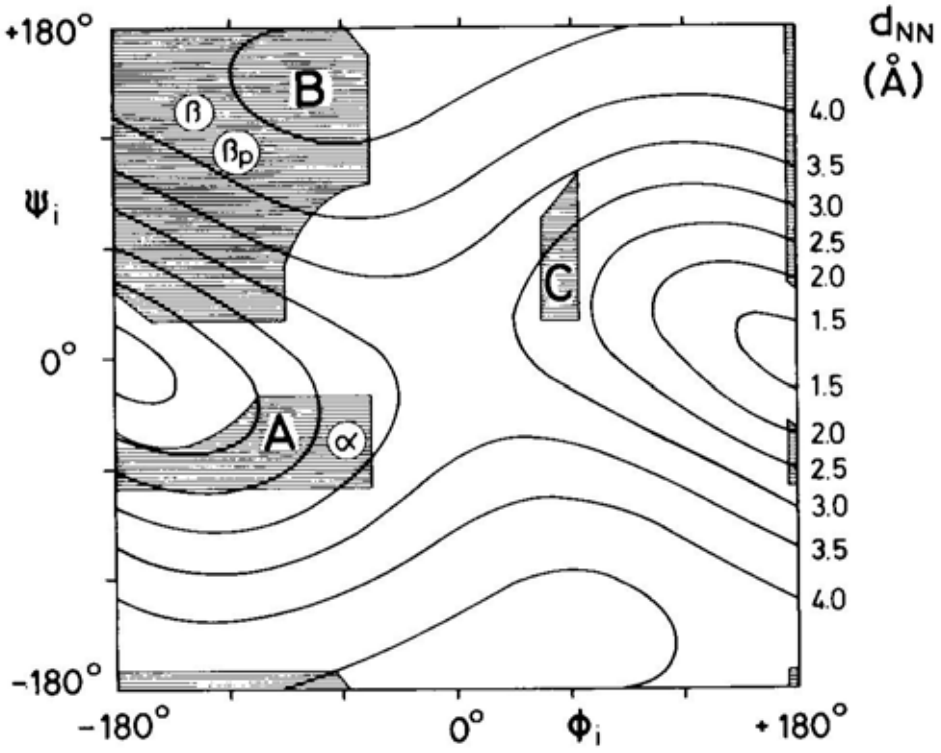

Figure 7.7. Sequential distance d_{NN} in the ϕ_i–ψ_i plane; solid contour lines represent fixed values of d_{NN} as indicated on the right. The shaded areas A, B, and C are sterically allowed for an alanyl dipeptide (Ramachandran and Sasisekharan, 1968). α, β, and β_p indicate the ϕ_i–ψ_i combinations for the regular α helix, antiparallel β sheet, and parallel β sheet (from Billeter et al., 1982).

Structural information deduced from solid state NMR spectroscopy

- Secondary shifts $\Delta\delta \equiv \delta_{fibril} - \delta_{coil}$ are strongly correlated with peptide or protein backbone conformation. In particular, values for β-strand segments are characteristically negative for $^{13}C_{\alpha}$ and ^{13}CO sites and positive for $^{13}C_{\beta}$ sites.

- Multiplicity of chemical shifts was attributed to the differences in molecular structure associated with the differences in fibril morphology.

- ^{13}C chemical shifts for D23, V24, G25 and G29 are inconsistent with expectations for a β-strand. Thus, the chemical shift data qualitatively suggest a conformation for the structurally ordered part of $A_{\beta 1\text{-}40}$ consisting of two β-strands that are separated by a bend or loop contained within residues 23-29. The conformation in the bend segment may vary with fibril morphology and fibrillization conditions.

- Linewidths in the 1.5-2.5 ppm range in solid state ^{13}C MAS NMR spectra are characteristic of well-structured peptide in rigid noncrystalline environments, whereas significantly larger linewidths are observed in disordered biopolymers shows that the N-terminal segment of $A_{\beta 1\text{-}40}$ is disordered in the fibrils.

- ^{13}C chemical shifts for CO, C_{α} and C_{β} sites and ^{15}N chemical shifts for backbone amide were analyzed to predict the backbone torsion angles for each residue. Predictions for two different choices of chemical shifts values are derived. Both lead to $\phi = -135^{\circ} \pm 25^{\circ}$ and $\psi = 140^{\circ} \pm 20^{\circ}$, consistent with a β-strand conformation, for all residues in the 9-21 and 30-36 segments. Non-β-strand ϕ and ψ values occur at D23, G25 and G29.

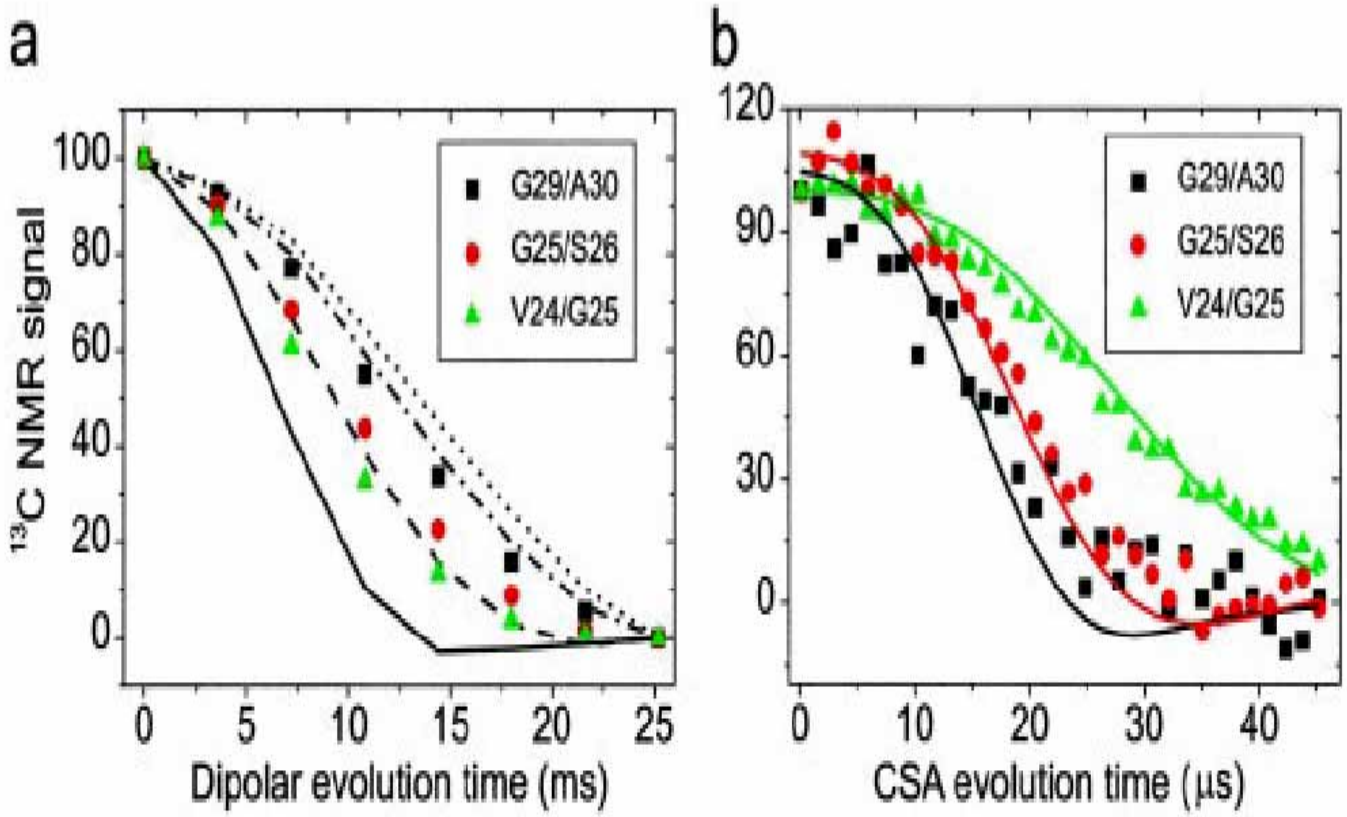

Fig. 3. Solid state NMR data on DLn Aβ_{1-40} fibril samples with ^{13}C labels at the indicated backbone carbonyl sites. These data constrain the ϕ and ψ angles of the second labeled residue. (*a*) fpRFDR-CT data and simulations for $\phi = 40°$ (solid line), 80° (dashed line), 120° (dot-dashed line), and 160° (dotted line). Simulations are scaled and baseline-corrected to match the first and last experimental data points. (*b*) DQCSA data and simulations for ϕ, $\psi = -70°$, $-40°$ (green); 70°, $-65°$ (red); and $-165°$, 135° (black).

Structural information deduced from solid state NMR spectroscopy

- Linewidths in the 1.5-2.5 ppm range in solid state ^{13}C MAS NMR spectra are characteristic of well-structured peptide in rigid noncrystalline environments, whereas significantly larger linewidths are observed in disordered biopolymers shows that the N-terminal segment of $A_{\beta 1\text{-}40}$ is disordered in the fibrils.

- ^{13}C chemical shifts for CO, C_α and C_β sites and ^{15}N chemical shifts for backbone amide were analyzed to predict the backbone torsion angles for each residue. Predictions for two different choices of chemical shifts values are derived. Both lead to $\phi = -135^\circ \pm 25^\circ$ and $\psi = 140^\circ \pm 20^\circ$, consistent with a β-strand conformation, for all residues in the 9-21 and 30-36 segments. Non-β-strand ϕ and ψ values occur at D23, G25 and G29.

- In RFDR-CT measurements, the decay of ^{13}C NMR signals from the labeled carbonyl sites reflects the strength of ^{13}C-^{13}C dipole-dipole couplings, which depends primarily on the intramolecular ^{13}C-^{13}C distance and hence the ϕ angle. In DQCSA measurements, the decay of ^{13}C NMR signals from the labeled sites reflects the relative orientation of the labeled carbonyl groups, which depends on both ϕ and ψ. The RFDR-CT and DQCSA data for different samples are significantly different, indicating significant differences in . Qualitatively, this result indicates the presence of non-β-strand conformations.

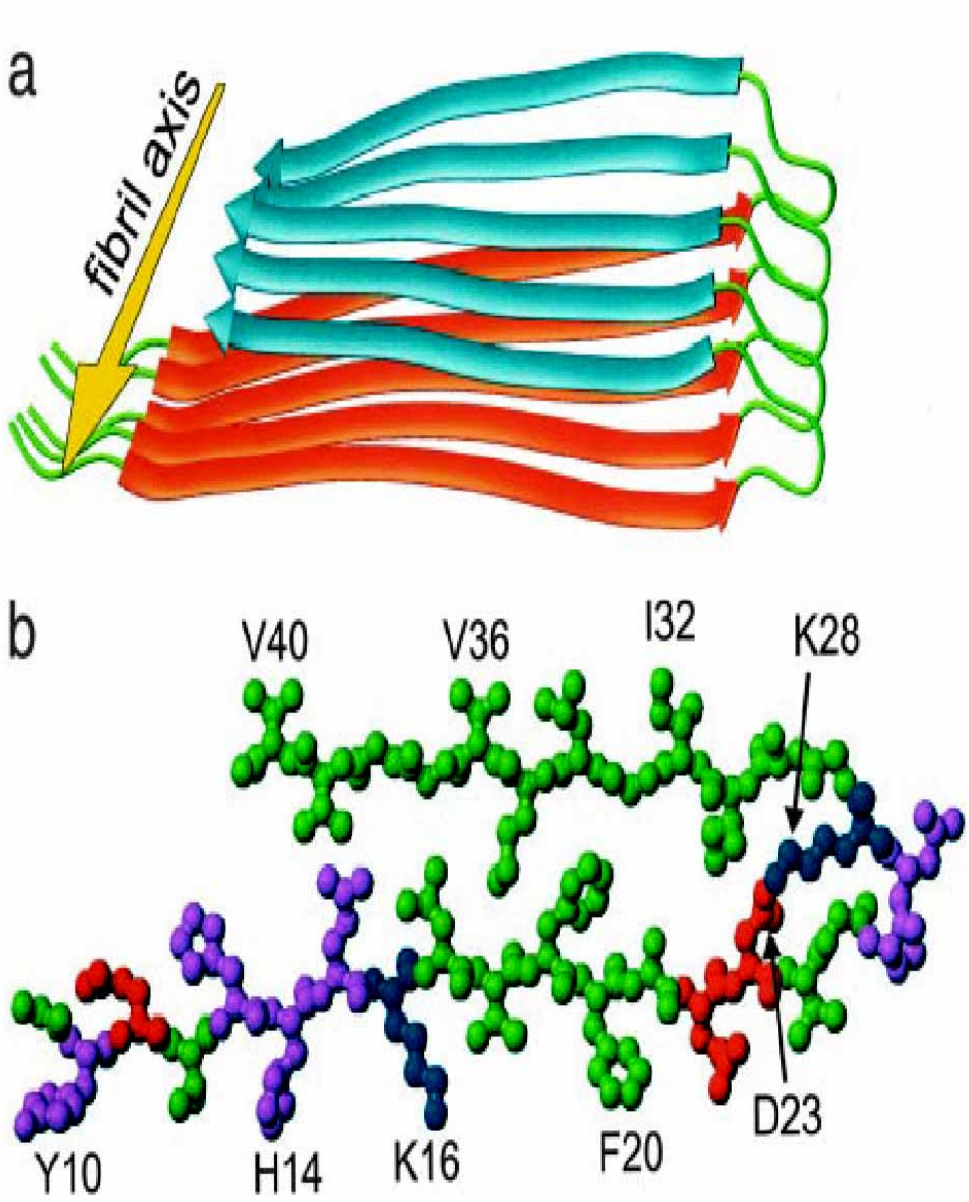

Fig. 4. Structural model for $A\beta_{1-40}$ fibrils, consistent with solid state NMR constraints on the molecular conformation and intermolecular distances and incorporating the cross-β motif common to all amyloid fibrils. Residues 1–8 are considered fully disordered and are omitted. (*a*) Schematic representation of a single molecular layer, or cross-β unit. The yellow arrow indicates the direction of the long axis of the fibril, which coincides with the direction of intermolecular backbone hydrogen bonds. The cross-β unit is a double-layered structure, with in-register parallel β-sheets formed by residues 12–24 (orange ribbons) and 30–40 (blue ribbons). (*b*) Central $A\beta_{1-40}$ molecule from the energy-minimized, five-chain system, viewed down the long axis of the fibril. Residues are color-coded according to their sidechains as hydrophobic (green), polar (magenta), positive (blue), or negative (red).

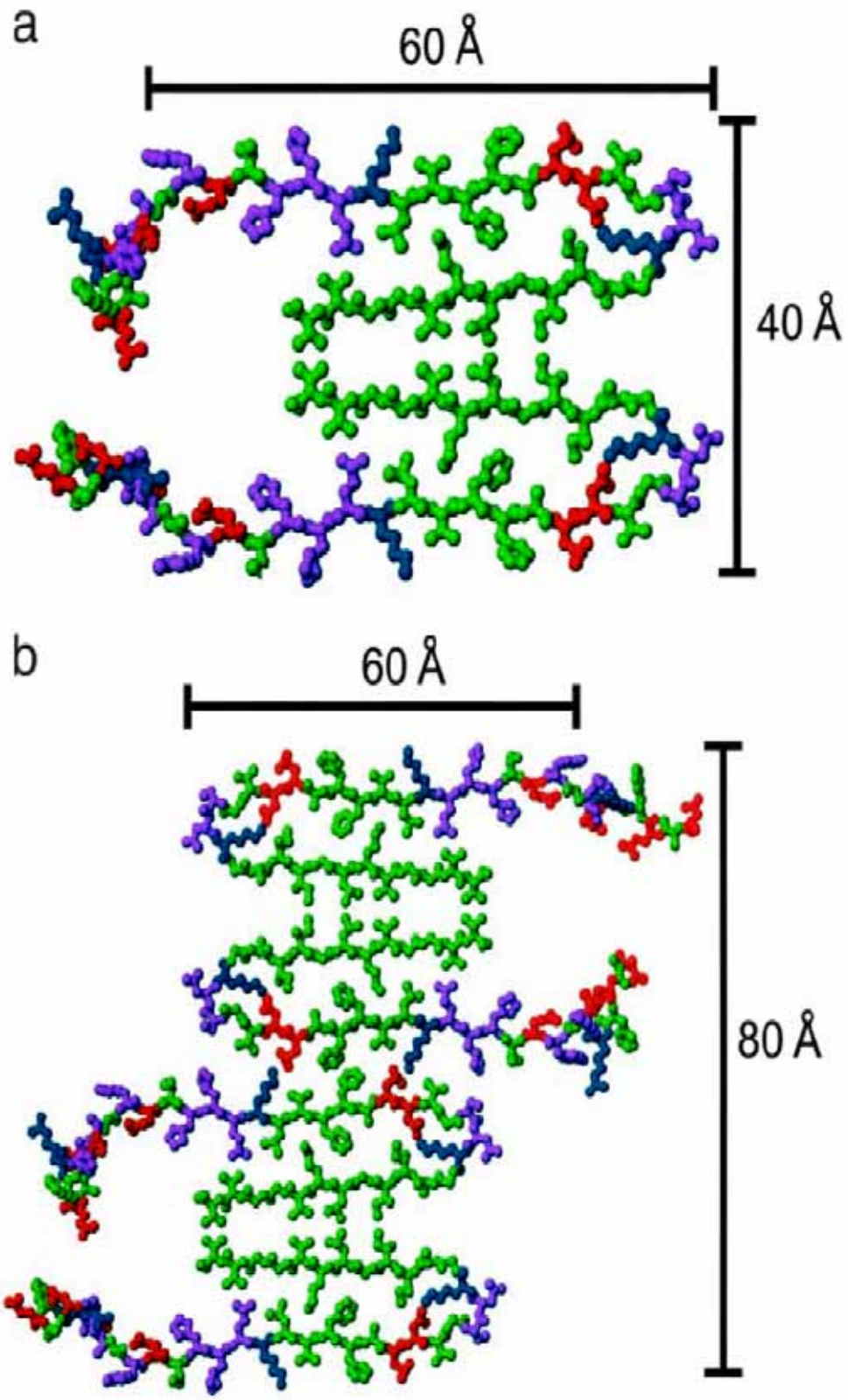

Fig. 5. (*a*) Cross section of an Aβ_{1-40} fibril with the minimal MPL indicated by scanning transmission electron microscopy (13, 29), formed by juxtaposing the hydrophobic faces of two cross-β units from Fig. 4. Residues 1–8 are included with randomly assigned conformations. (*b*) Possible mode of lateral association to generate fibrils with greater MPL and greater cross-sectional dimensions.